Oil & Gas Science and Technology – Rev. IFP Energies nouvelles **74**, 86 (2019)

https://doi.org/10.2516/ogst/2019056

Available online at:
ogst.ifpenergiesnouvelles.fr

REGULAR ARTICLE OPEN ACCESS

The effect of impurity on miscible CO_2 displacement mechanism

Erhui Luo[1,*], Yongle Hu[1], Jianjun Wang[1], Zifei Fan[1], Qingying Hou[1], Liangtao Ma[2], and Shuhui Dai[3]

[1] PetroChina Research Institute of Petroleum Exploration & Development, Beijing 100083, China
[2] CNOOC Research Institute Company Limited, Beijing 100028, China
[3] China ZhenHua Oil Company Limited, Beijing 100031, China

Received: 26 August 2019 / Accepted: 14 October 2019

Abstract. The CO_2 displacement is one of the gasflooding Enhanced Oil Recovery (EOR) methods. The application from volatile oil to black oil is popular mainly because CO_2 requires a relatively low miscibility pressure, which is suitable to most reservoir conditions. However, CO_2 always contains some impurity, such as CH_4, H_2S and N_2, leading to the change of phase behavior and flooding efficiency. Whether the gasflooding achieves successfully miscible displacement depends on the reservoir pressure and temperature, injected solvent and crude oil compositions. So three different types of oil samples from the real field are selected and mixtures of CH_4, H_2S and N_2 with various CO_2 concentrations as the solvent are considered. After a series of experimental data are excellently matched, three nine-pseudocomponent models are generated based on the thermodynamic Equation-of-State (EoS), which are capable of accurately predicting the complicated phase behavior. Three common tools of pressure–temperature (P–T), pressure–composition (P–X) and pseudoternary diagrams are used to display and analyze the alteration of phase behavior and types of displacement mechanism. Simulation results show that H_2S is favorable to attain miscibility while CH_4 and N_2 are adverse, and the former can reduce the Multiple Contact Miscibility (MCM) pressure by the maximum level of 1.675 MPa per 0.1 mol. In addition, the phase envelope of the mixtures CO_2/H_2S displacing the reservoir oil on the pseudoternary diagram behaves a triangle shape, indicating the condensing-dominated process. While most phase envelopes of CO_2/CH_4 and CO_2/N_2 exhibit the trump and bell shapes, revealing the MCM of vaporization.

1 Introduction

The CO_2 flooding has achieved many successful applications of field projects around the world (Babadagli, 2007; Luo *et al.*, 2013a, b; McGuire *et al.*, 2017). Because the displacement process that CO_2 is injected into the subsurface not only can Enhance Oil Recovery (EOR) but also storage CO_2 in order to reduce greenhouse gases discharge. Generally, the CO_2 drive is one of the effective gasflooding methods that attain higher recovery than waterflooding, in particular the miscible displacement condition of approaching 100% oil recovery in the swept area. The reason why CO_2 is preferably selected as an EOR injectant is that the crude oil would be swollen and promoted a reduction of viscosity, with requirement of relatively low miscible pressure (Abdurrahman *et al.*, 2015; Han *et al.*, 2016; Hand and Pinczewskl, 1990; Simon and Graue, 1964; Rahimi *et al.*, 2017; Stalkup, 1987; Tsau *et al.*, 2010; Yang *et al.*, 2009). Essentially three types of displacement processes in a CO_2 injection process can be defined as shown in Figure 1a: immiscible, near miscible and miscible. The miscible drive is further classified as First-Contact Miscibility (FCM) and Multiple Contact Miscibility (MCM) on the basis of interphase mass transfer mechanism (Al-Wahaibi *et al.*, 2007; Coats *et al.*, 2007). The MCM process includes three mechanisms: condensing gas drive corresponding to backward contacts, vaporizing gas drive corresponding to forward contacts, and a combination of condensing/vaporizing gas drive (Zick, 1986). As can be seen in Figure 1b, for different processes of CO_2 displacing crude oil, the immiscible flooding is formed a distinct interface of two-phase between gas zone and oil zone, leaving more residual oil saturation. Among these processes, the FCM displacement yields a single-phase transition zone separating the injected solvent from the crude oil, and is piston-like with the most efficient recovery. The MCM drive is analogous to near miscible process. The vaporization zone of intermediate components and extraction zone of C5 through C30 are developed, which results in residual saturation lower than immiscibility but greater than FCM (Holm and Josendal, 1974; Wang, 1986).

However, pure CO_2 with 100% concentration is almost impossible. Regardless of the separation from the oil and gas industry or the capture from other sources, CO_2 always contains some impurities, such as CH_4, H_2S and N_2 (Belhaj *et al.*, 2013a; Chapoy *et al.*, 2013; Jin *et al.*, 2018; Li *et al.*,

* Corresponding author: luoerhui2006@163.com

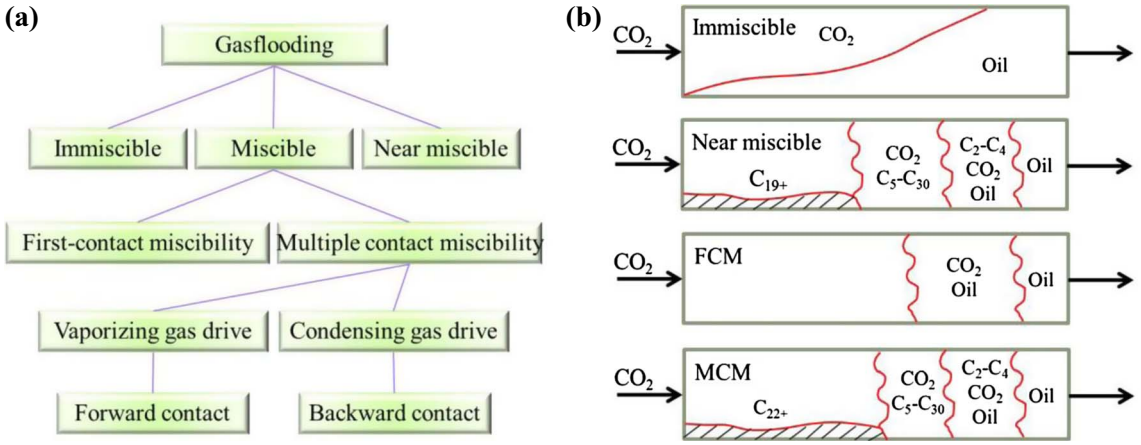

Fig. 1. (a) Classification of displacement process for gasflooding, (b) schematic of various types of CO_2 displacement.

2011; Ziabakhsh-Ganji and Kooi, 2012). The mixture of CO_2 and H_2S is so-called acid gas. The concept of acid gas is different from sour gas which consists of natural gas and a high H_2S content. The sour gas reservoirs that are discovered all over the world are the main sources of acid gas (Abou-Sayed *et al.*, 2004; Behrend *et al.*, 2007; Huang *et al.*, 2011; Onerhime *et al.*, 2014; Mohsen-Nia *et al.*, 1993; Verlaan and Zwet, 2012). The research on acid gas as a flooding agent of EOR has received wide interest since the 1960s (Battistelli and Marcolini, 2009; Harvey and Henry, 1960; He *et al.*, 2019; Luo *et al.*, 2019a, b; Siddiqui *et al.*, 2013; Trivedi *et al.*, 2005; Vark *et al.*, 2004). Besides, the disposal of acid gas that is injected into the reservoir is also a concern (AlFalahy *et al.*, 1998; Bachu and Gunter, 2005; Longworth *et al.*, 1996). The previous work indicated that H_2S is an effective solvent and requires lower miscibility pressure than CO_2. But the toxicity of H_2S limits its widespread application. On the other hand, the mixture of CO_2 and N_2, so-called flue gas, is used to drive the crude oil for EOR and receives extensive attention (Abrishami and Hatamian, 1996; Bahralolom and Orr, 1988; Belhaj *et al.*, 2013b; Fandino *et al.*, 2015; Firoozabadi and Aziz, 1986; Srivastava and Huang, 1997). In a word, the presence of CH_4, H_2S and N_2 in the CO_2 stream alters phase behavior of the reservoir oil and injected gas system, which influences extremely displacement mechanism and recovery efficiency. Consequently, the knowledge of phase behavior and displacement mechanism of various mixtures of CO_2/CH_4, CO_2/H_2S and CO_2/N_2 as injected solvents is required.

At least there are three existing techniques to describe the vapor/liquid phase behavior of mixtures of the crude oil and injected gas: pressure–temperature (P–T), pressure–composition (P–X), and pseudoternary diagrams. These diagrams provide some very useful information to identify the single- or multi-phase states, calculate FCM and MCM pressures, and determine the condensing-gas drive or vaporizing-gas drive mechanism. In general, the P–T diagram is a frequently used approach to identify types of the reservoir fluid. Based on the temperature range of the abscissa, five regions are often divided representing black oil, volatile oil, condensate, wet gas and dry gas, respectively, from the left to the right of the x-axis on the P–T diagram. The P–X diagram can offer a quick evaluation of FCM in a swelling test, and also recognize types of reservoir fluids. In particular, the pseudoternary diagram is helpful in accounting for the development of miscibility in a multiple contact process of a multicomponent system. Success in miscibility development in the reservoir condition depends on an understanding of phase behavior. In turn, the phase behavior of a system depends on the reservoir temperature, pressure, and compositions of the crude oil and the injected gas, which determines the final displacement efficiency.

The purpose of this work is to examine the effect of impurity on the CO_2 displacement mechanism and phase behavior by utilizing various techniques of P–T, P–X and pseudoternary diagrams. Three types of representative reservoir oil samples are used for various CO_2 mixtures flooding. After detailed matching PVT experiments, three nine-pseudocomponent fluid models with high accuracy are established for subsequent investigations. Various binary mixtures of CO_2 with CH_4, H_2S and N_2 gases in different proportions are selected as the injected solvent. Both the change of phase behavior and the description of miscible mechanism are displayed illustratively by on the use of three tools of P–T, P–X and pseudoternary diagrams.

2 EOS-based phase behavior modeling

The study of phase behavior is a key of understanding the gas injection process, especially miscible displacement mechanism. Both PVT laboratory experiments and compositional simulation are necessary to establish complicated phase behavior (Neau *et al.*, 1993; Jaubert *et al.*, 1995; Luo *et al.*, 2013c). Figure 2 shows the procedure of phase behavior study in our work. To begin with the conventional PVT measurements of three oils, such as Constant Composition Expansion (CCE), Constant Volume Depletion (CVD)

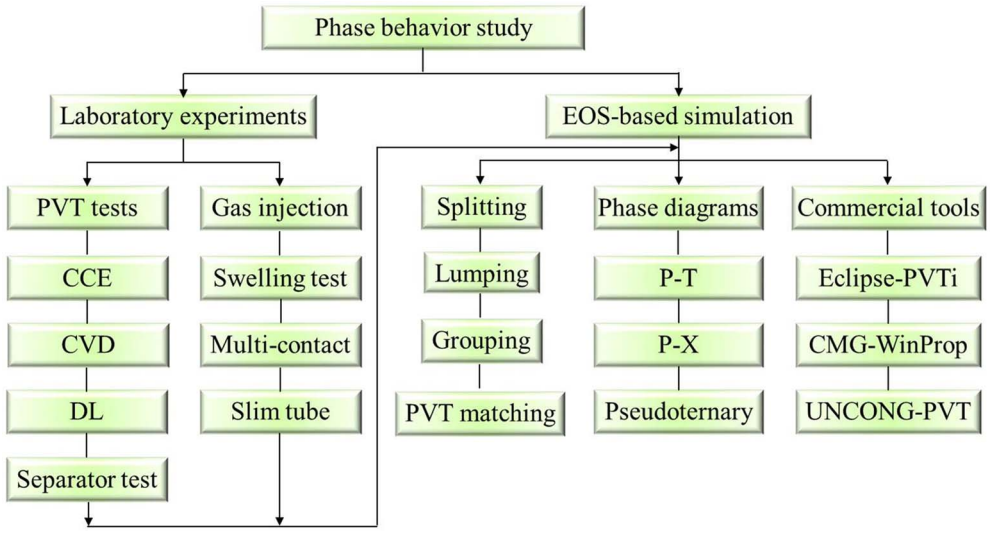

Fig. 2. Procedure of phase behavior study.

and Differential Liberation (DL), then an Equation-of-State (EoS)-based compositional model is built to match experimental data. Finally, the generated thermodynamic parameters with proper adjustment are used to run compositional simulation.

2.1 Fluid description

The accuracy of PVT experimental data depends on the quality of the oil sample. In order to keep the reservoir oil as a single phase above the saturation pressure, three representative oils are from downhole sampling. Among these three oil samples, both Kash and Ken samples are from the carbonate reservoir of Pre-Caspian basin and the Jilin sample is from the sandstone reservoir of Songliao basin in China. Both Kash and Jilin samples are extended compositional analysis up to C36+ fraction while the Ken only up to C11+ fraction. The plus fraction properties are as follows:

Kash C36+: Mw = 550 and SG = 0.927; Ken C11+: Mw = 290 and SG = 0.855; and Jilin C36+: Mw = 675 and SG = 0.866.

The multicomponent mixtures of three samples used should first be represented approximately by three pseudocomponents of pseudoternary diagrams: CH_4 and N_2 representing a light pseudocomponent, C2–C6 and nonhydrocarbons of CO_2 and H_2S representing an intermediate pseudocomponent, and C7+ representing a heavy hydrocarbon pseudocomponent. The three apexes of the diagram represent 100% content of the three pseudocomponents, respectively. In this approach of specifying grouping, three fluids of Kash, Ken and Jilin under the reservoir pressure and temperature conditions are plotted on the pseudoternary diagram by the circle with marked different colors in Figure 3. In order to enhance the comparison, the typical condensate and gas data from the literature (Spivey and McCain, 2013) are also plotted on the diagram. Obviously, both the condensate and gas are close to the apex of CH_4 and N_2. However, both Kash and Ken oils lie in the red

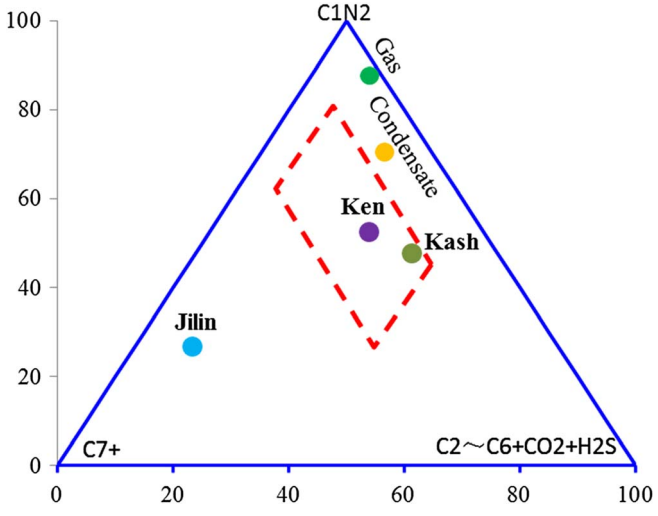

Fig. 3. Pseudoternary diagrams for oil samples and typical gases.

dashed line quadrangle that belongs to the volatile oil region. The Jilin oil containing 63.2% C7+ lies in the black oil region because of approaching the apex of heavy pseudocomponent. In addition, the Kash oil contains H_2S and CO_2 mole percent larger than 19%. As a result, three different oil samples are defined as: sour volatile oil (Kash), volatile oil (Ken) and black oil (Jilin). Noted that all subsequent pseudoternary diagrams chose this representation manner as a basis for comparing and analyzing.

2.2 Grouping

The purpose of grouping is to reduce the number of components of reservoir oils and save computation time of compositional simulation. Because the plus fraction would yield

Table 1. Thermodynamic properties of pseudocomponents for three oil samples.

Sample	Component	P_c (atm)	T_c (K)	ω	Mw (kg/mol)	Z_c	V_c (L/mol)	T_b (°C)	Parachor
Common part	H_2S	88.2	373.2	0.1	34	0.285	0.099	−60.4	80
	CO_2	72.8	304.2	0.225	44	0.274	0.094	−78.5	78
	N_2	33.5	126.2	0.04	28	0.291	0.090	−195.8	41
	CH_4	45.4	190.6	0.008	16	0.288	0.099	−161.5	77
Kash	C2–C3	45.9	330.4	0.118	35	0.278	0.167	−56.7	123
	C4–C6	34.8	456.7	0.225	69	0.272	0.292	31.3	215
	C7–C12	32.6	588.3	0.558	121	0.294	0.473	146.2	347
	C13–C22	21.7	721.5	0.687	223	0.286	0.835	286.8	596
	C23–C36+	10.4	703.1	1.285	401	0.258	1.406	452.2	915
Ken	C2–C3	45.5	333.9	0.120	36	0.278	0.170	−53.3	126
	C4–C6	34.4	462.0	0.231	71	0.272	0.298	35.4	220
	C7	24.5	570.5	0.356	96	0.230	0.381	92.9	278
	C8–C10	21.1	577.0	0.795	124	0.236	0.485	150.0	356
	C11+	18.0	663.1	1.011	290	0.306	1.165	368.3	740
Jilin	C2–C3	46.3	326.5	0.114	34	0.278	0.164	−60.8	121
	C4–C6	34.0	469.3	0.240	73	0.271	0.304	39.8	226
	C7–C12	25.2	577.0	0.430	132	0.267	0.514	164.8	376
	C13–C22	20.7	684.2	0.578	233	0.291	0.869	297.2	617
	C23–C36+	10.3	721.5	0.937	477	0.280	1.649	475.1	979

large error. The components C36+ of Kash and Jilin and C11+ of Ken are first characterized by Twu correlation to calculate critical properties based on the input of Mw and SG. Considering the injected gas including CO_2, H_2S, CH_4, N_2 and their mixtures, the four pure compounds are treated as individual component. The common part of Table 1 gives their critical properties as constant. Also, two pseudocomponents are generally adequate to the intermediate components of C2–C6. To keep the same number of pseudocomponents, the C7+ fractions are grouped into three pseudocomponents. For Kash and Jilin oils, the three groups of C7–C12, C13–C22 and C23–C36+ are proposed according to Whitson's grouping procedure. However, the equal mole fraction method (Newley and Merrill, 1991) for Ken oil is more appropriate, with three groups of C7, C8–C10 and C11+ presented. Finally, a nine-pseudocomponent grouping scheme is determined.

2.3 PVT experimental matching

The validation of the EOS-based nine-pseudocomponent model by experimental data is crucial to predict accurately phase behavior. The three-parameter PR-EOS with good accuracy (Li and Yan 2009) is used to perform simulation runs. The classical Soave alpha-function is used for the cubic equation of state, and its first and second derivatives must exist and be continuous in order to obtain accurate and physically meaningful behavior through strictly mathematical analysis proposed by Le Guennec *et al.* (2016a, b). As a matter of fact, one probable solution to guarantee the α-function consistent is adjusting the acentric factor to match experimental data from a reservoir engineering point of view. These four parameters of three heavy pseudocomponents incorporating the critical pressure (P_c), critical temperature (T_c), acentric factor (ω) and critical volume (V_c) are selected as tuning variables. The following section presents the matching results.

2.3.1 Kash sour volatile oil

The tests of CCE, CVD and DL are performed for Kash oil. At the reservoir temperature of 109 °C, the saturation pressure of the fluid is determined to be 28.9 MPa from the CCE test when the relative volume reaches 1. The first step is to match the saturation pressure by tuning P_c, T_c and ω, and the weight value is set to 10. The simulated value of saturation pressure is 29.72 MPa, with the relative error of 0.0284 acceptable. The second step is to match oil density with the weight of 2 by adjusting the volume translation. This parameter mainly improves predictions of the liquid density as a correction term (Jaubert *et al.*, 2016; Privat *et al.*, 2016). Moreover, the binary interaction coefficients are changed by adjusting the critical volumes. The third step is to match oil viscosity by tuning polynomial coefficients of Jossi–Stiel–Thodos correlation. At the same time, the mole recovery and liquid saturation of CVD test and GOR of DL test are also adjusted automatically. Figures 4 and 5 show a good match between experimental data and simulation calculations. Figure 6 presents a comparison result of pre-match and post-match of P–T diagrams. The main difference is that the size of two-phase region becomes small after experiment matching.

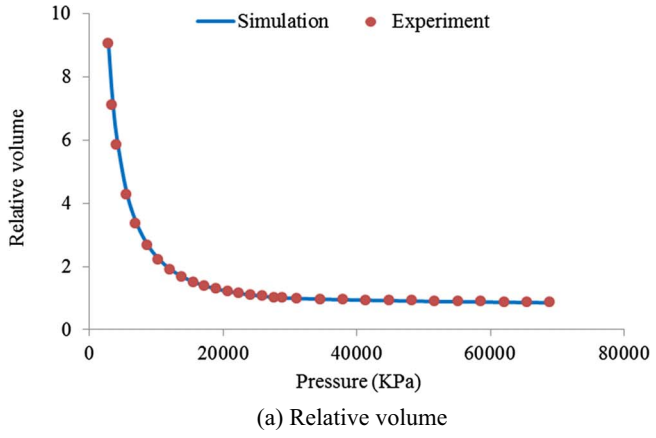

(a) Relative volume

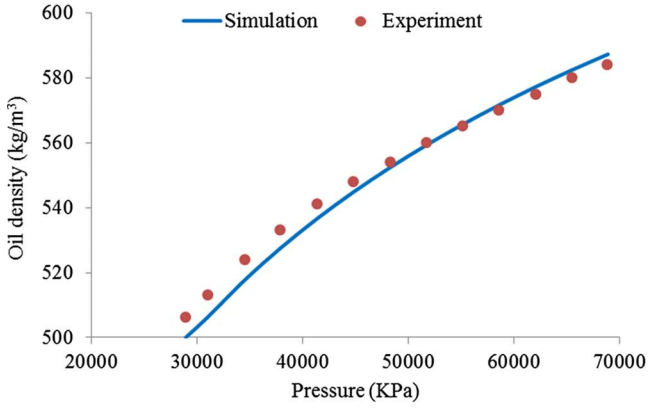

(b) Oil density

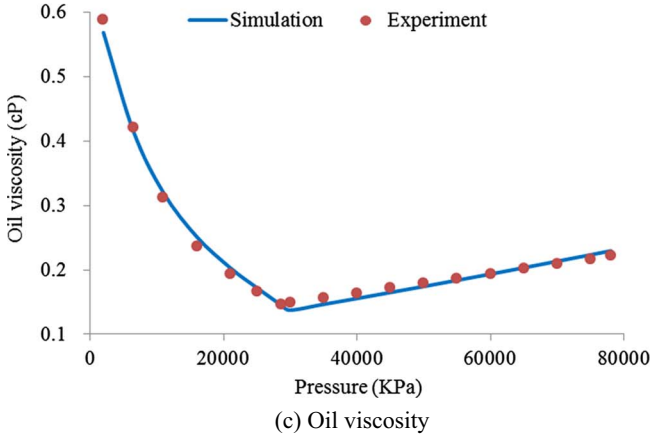

(c) Oil viscosity

Fig. 4. Comparison of experimental measurements and PVT simulation results for CCE tests.

2.3.2 Ken volatile oil

The Ken oil also provides CCE, CVD and DL measurements but is lack of oil density and liquid saturation parameters. The saturation pressure at 91.7 °C is determined to be 30.1 MPa. The calculated saturation pressure is equal to 30.02 MPa, with a small relative error of 0.0027. The similar procedure of tuning parameter is implemented, and the matching results are shown in Figures 7 and 8, exhibiting an excellent matching. Similarly, on the P–T phase diagram,

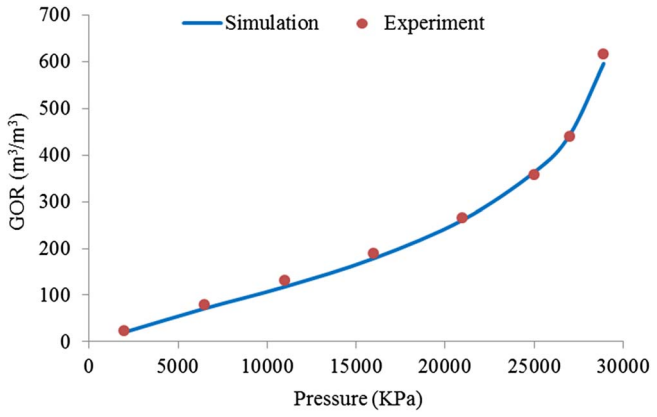

Fig. 5. Comparison of experimental measurements and PVT simulation results for DL tests.

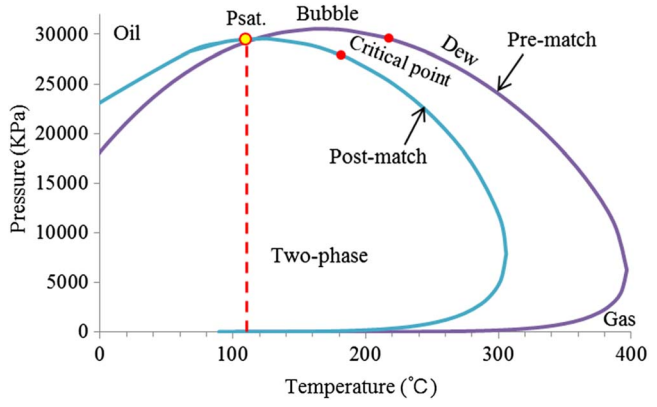

Fig. 6. Comparison of pre-match and post-match results for pressure–temperature phase diagrams.

the phase envelope of post-match is contracted compared to pre-match as shown in Figure 9.

2.3.3 Jilin black oil

The Jilin oil only offers the CCE test. Therefore, the three physical properties of relative volume, oil density and oil viscosity are matched as shown Figure 10. The saturation pressure at 108.4 °C is determined to be 10.41 MPa. The matching saturation pressure is 10.419 with a small relative error of 0.0009. On the P–T diagram in Figure 11, it is obvious that the saturation pressure of pre-match is higher than that of post-match.

Finally, Table 2 summarizes all the Absolute Average Error (AAE) between experimental data and simulated data of the EOS model, where AAE is defined as $\mathrm{AAE} = \sum_{i=1}^{N} \frac{X^i_{\mathrm{exp}} - X^i_{\mathrm{sim}}}{X^i_{\mathrm{exp}}} / N$. The maximum AAE is 0.0492, which is acceptable in the reservoir engineering. After the verification of the PR-EOS model against PVT laboratory experiments, three nine-pseudocomponent models are generated for the three fluids, respectively. Table 1 gives the thermodynamic properties of each pseudocomponent used for multicomponent simulations.

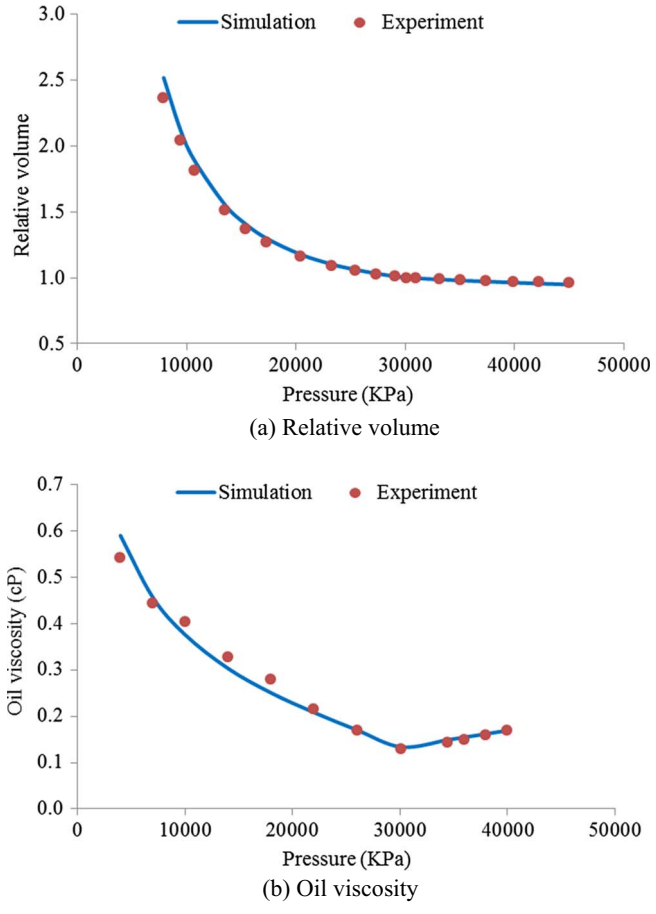

Fig. 7. Comparison of experimental measurements and PVT simulation results for CCE tests.

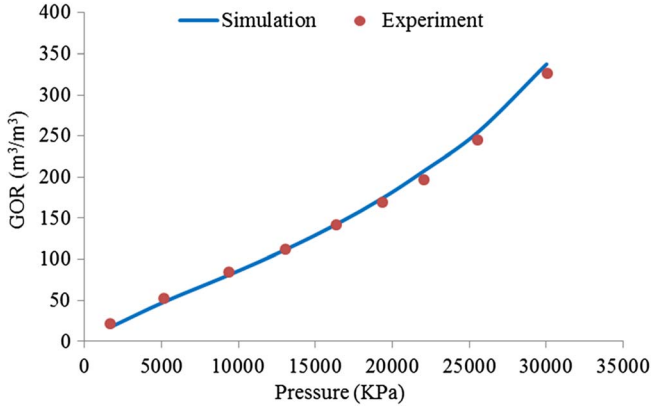

Fig. 8. Comparison of experimental measurements and PVT simulation results for DL tests.

3 Effect of impurity on displacement mechanism

In order to study the effect of impurity in the injecting CO_2 stream on displacement mechanism, three types of gas and various proportion mixtures with CO_2 are chosen. According to the pure gas P–T diagram, it has been recognized that N_2 and CH_4 have lower temperature range compared to CO_2 and H_2S, which means that CO_2 and H_2S can readily be liquefied at relatively high temperatures during gas injection process. The following section gives the detailed results of phase behavior and displacement mechanism of three reservoir oils (Kash, Ken and Jilin).

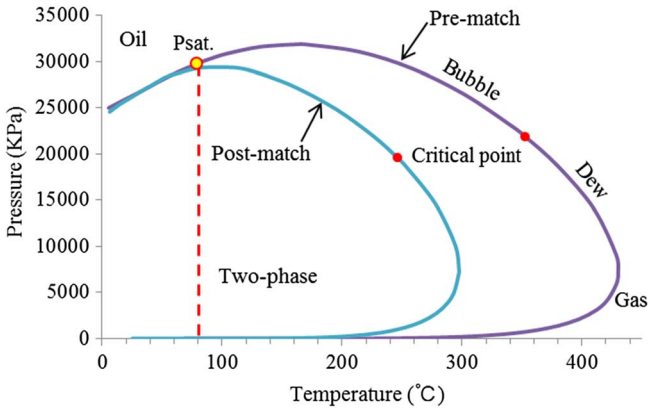

Fig. 9. Comparison of pre-match and post-match results for pressure–temperature phase diagrams.

3.1 Evaluation on sour volatile oil

3.1.1 P–T consideration

For a gas injection flooding, the change of phase behavior can be directly seen by examining a P–T diagram. Figure 12a shows how the phase boundary curve might vary with the injection CO_2 mole fraction for the Kash sour volatile oil. Apparently increasing CO_2 mole fraction reduces gradually the size of the two-phase region, and both the bubble point curve and dew point curve become retractable. At the same time, the critical point moves toward to the left of the P–T plot. The shrinking feature of two-phase region indicates that injecting more CO_2 would lead to readily attain miscibility. The other gas, such as H_2S, CH_4 and N_2, is added to the Kash reservoir oil, displayed the phase behavior relations in Figure 12b. As can be seen, the bubble point curves of CO_2 and H_2S have the retractable characteristic while those of CH_4 and N_2 have the expanding trend. As a result, the two-phase region becomes more and more larger from the minimum H_2S to the maximum N_2. The qualitative description of P–T diagram demonstrates that a higher pressure is required for achieving miscible displacement with CH_4 and N_2 than with CO_2 and H_2S.

3.1.2 CO_2/CH_4

A series of simulation calculations of swelling test are performed. Figures 18a and 18b show the saturation pressure and swelling factors for the Kash oil at 109 °C, respectively, where the mixture composition on the abscissa is

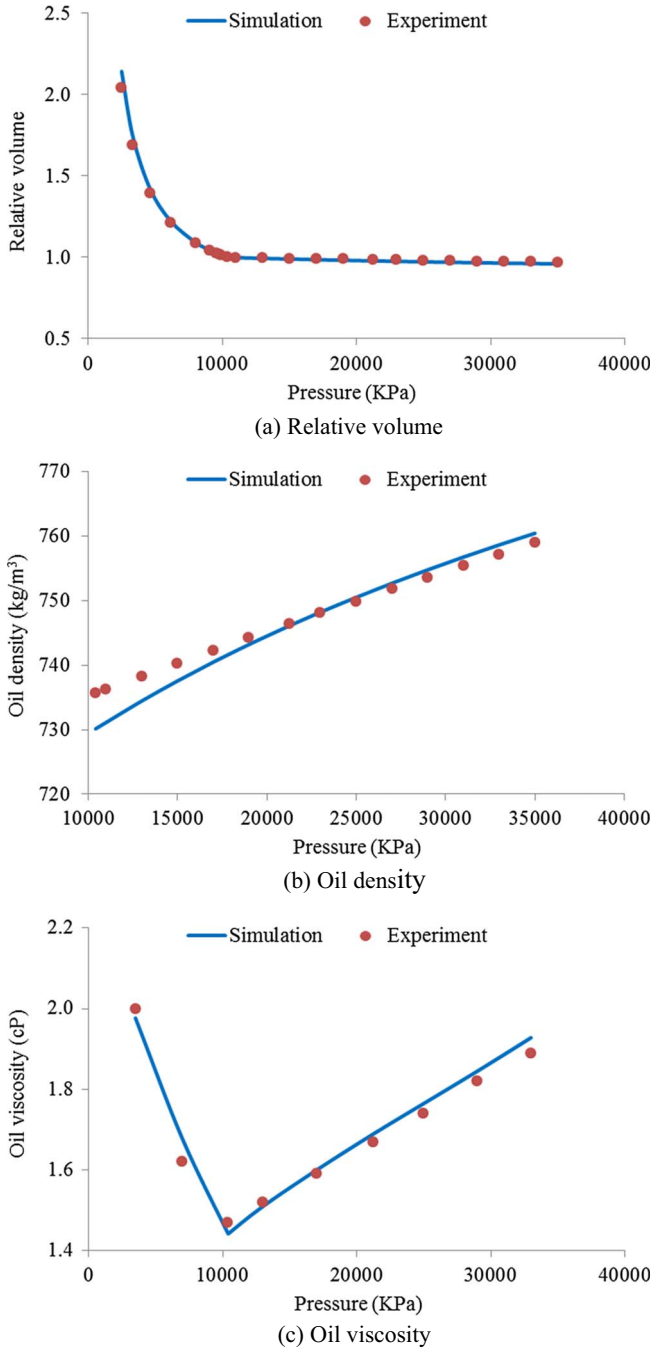

Fig. 10. Comparison of experimental measurements and PVT simulation results for CCE tests.

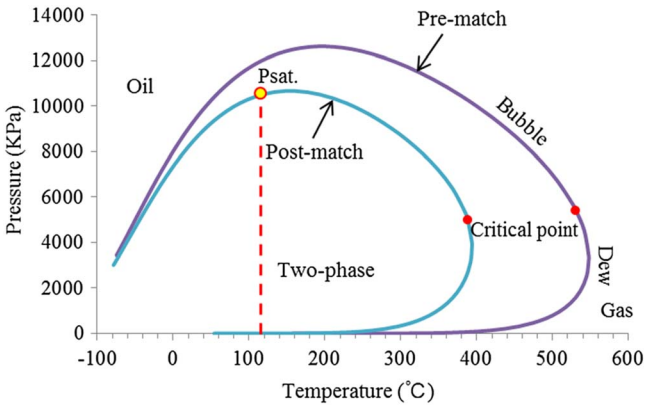

Fig. 11. Comparison of pre-match and post-match results for pressure–temperature phase diagrams.

expressed as a mole fraction of the injected binary gas CO_2/CH_4. In Figure 13a, the trend of saturation pressure increases then decreases with the increase of injected CO_2/CH_4 gases except pure CO_2. On the other hand, the higher the CH_4 concentration, the larger the saturation pressure becomes. Because initially as injection gas is added to the reservoir oil, this system exhibits bubble points at the saturation pressure. Further additions of the injected gas CO_2/CH_4 give dew points. However, pure CO_2 mixed with the Kash oil would result in the monotonic reduction of saturation pressures. The reason is that pure CO_2 injection is a condensing/vaporizing gas drive process while CO_2 mixed with CH_4 injection is probable a vaporizing gas drive process. Another purpose of pressure-composition diagrams is to provide the simplest and most direct method to identify whether achieving miscible displacement or not. The cricondenbar on the P–X plot is called FCM pressure marked by red points that the injected gas would mix with the reservoir oil completely in all proportions by first-contact miscible flooding. Above the FCM pressure, all mixtures are kept in single phase. It is obvious that the higher CH_4 mole fraction, the larger FCM pressures become. Therefore, from the gas injection view, CH_4 has a negative effect on miscible CO_2-EOR.

From Figure 13b, when mixtures of CO_2/CH_4 dissolve in the Kash oil, a monotonic increase in liquid volume happens. This is so-called swelling effect. Obviously the swelling capability of CH_4 is lower than that of CO_2. The maximum swelling factor of pure CO_2 is 1.26 times as large as pure CH_4. In addition, the higher the CH_4 content, the smaller the swelling factor becomes. When the injected solvent reaches 0.8 mol, the maximum swelling factor exceeds 3.9 whatever the amount of CH_4. The injected gas raises extensively volumetric expansion of subsurface fluid, which is one of the main contributions to gas flooding EOR.

From the thermodynamics view, the pseudoternary diagram has the advantage of capturing the essence of miscible development. Consequently, the vaporizing and condensing gas drive processes represented in pseudoternary diagrams are simulated using a cell-to-cell method (Luo *et al.*, 2019b). Figure 14 shows simulated pseudoternary diagrams for pure CO_2 displacing the Kash oil at the reservoir temperature of 109 °C. The position of the red circle represents the Kash oil and the injected gas locates on the diamond. The two-phase boundary curve is composed of the dark red bubble point and green dew point curves. Firstly, the FCM is impossible for the given pressure and temperature conditions because the straight line connecting the Kash oil composition and CO_2 passes through the two-phase

Table 2. AAE for different matching experiments.

Experiment	Parameter	Kash	Ken	Jilin
CCE	Relative volume	0.0112	0.0163	0.0088
CCE	Oil density (kg/m^3)	0.0064	–	0.0027
CCE	Oil viscosity (cP)	0.0334	0.0425	0.0154
DL	GOR (m^3/m^3)	0.0481	0.0492	–

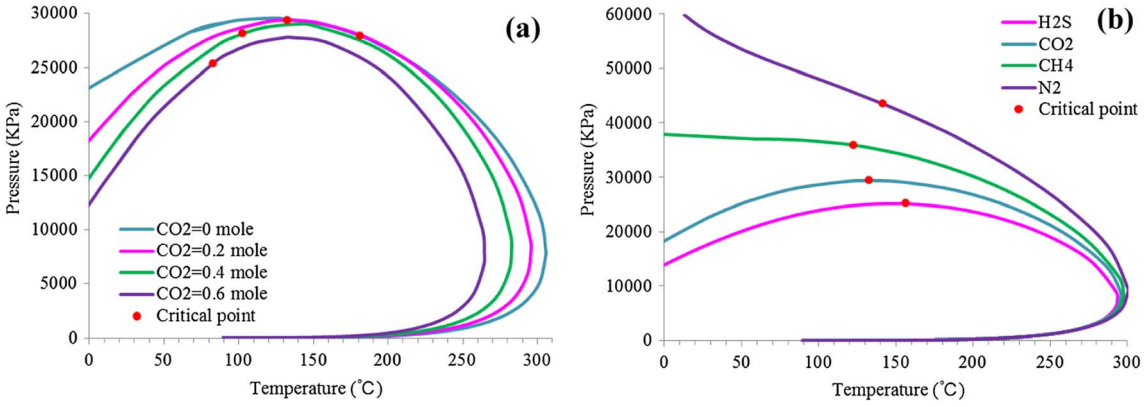

Fig. 12. Pressure–temperature diagrams for Kash sour volatile oil with (a) CO_2 mixtures and (b) various injected gases.

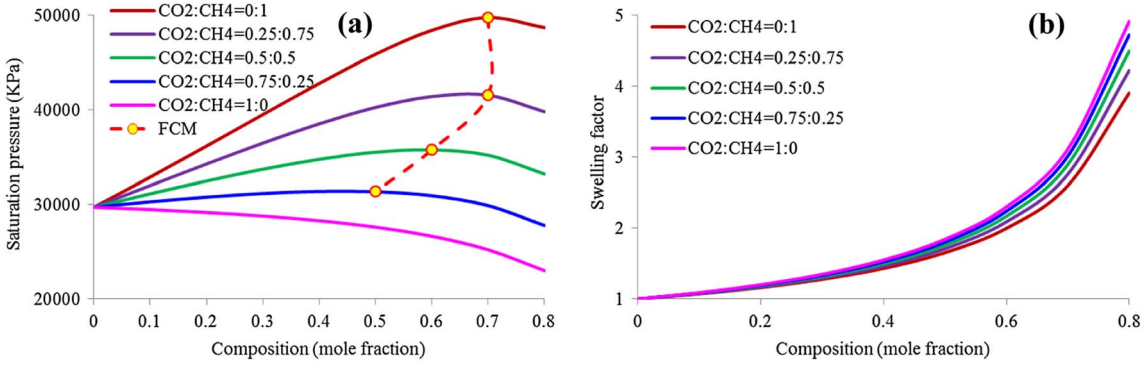

Fig. 13. (a) Pressure–composition diagrams and (b) swelling factors for Kash sour volatile oil and CO_2/CH_4 mixtures at 109 °C.

region. The next step is to calculate MCM pressure. As pressure is increased, the two-phase region constricts continuously. Noted that the phase envelope does not close at the joint of the bubble point and dew point curves, indicating MCM is not achieved. As the CO_2 gas continues to extract C5–C30 hydrocarbons and condensate the intermediate components of the reservoir oil, the liquid composition is modified progressively until it becomes miscible with the injection solvent. At the pressure of 26.25 MPa, the two-phase boundary curve generates an almost closed phase envelope, indicating CO_2 is miscible with the Kash oil by multiple backward contacts. The traditional interpretion of phase rule is not valid for condensing and extraction processes. The mechanism is also pointed out by Nutakki *et al.* (1991). Finally the phase envelope with achieving multicontact miscibility has a triangle shape. According to the simulation run, the condensation and extraction are the major mechanism responsible for the MCM process of pure CO_2. It is emphasized that sometimes the MCM may be attempted but not achieved, or unforeseen factors could destroy miscibility process.

Considering effect of CH_4 on the CO_2 flooding process, various proportions of CH_4 are mixed with CO_2 to gain binary solvents that are used to displace the reservoir oil. The pseudoternary diagrams are plotted in Figure 15. The calculated results clearly show that the shape of phase

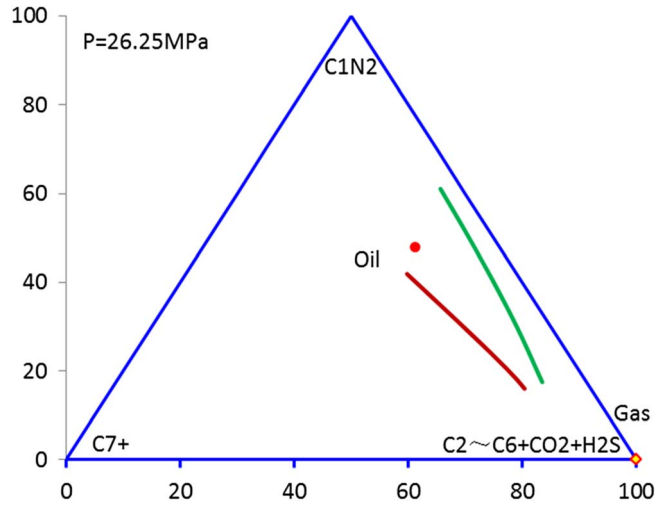

Fig. 14. Pseudoternary diagrams for Kash sour volatile oil sample at 109 °C with CO_2 as injection gas.

envelop differs absolutely from that of pure CO_2, with the appearance of the trump (Figs. 15a and 15b) and bell (Figs. 15c and 15d) shapes. The transformation of the shape would occur when CH_4 concentration exceeds certain level. The almost closure appears in Figure 15a and complete closures appear in Figures 15b–15d. The corresponding MCM pressures are 31.25, 31.875, 31.875 and 32 MPa over CH_4 content range from 0.25 to 1 mol fraction. According to the phase rule, as long as the crude oil composition lies to the right of the limiting tie line that is defined as the tangent to the phase envelope that passes through the plait point, the vaporization mechanism would be dominant. Thus it is simple to identify Figures 15b through 15d as the vaporizing gas drive. These figures further illustrate that the presence of CH_4 in a CO_2 displacement raises noticeably MCM pressures but the incremental magnitude is relatively small with increasing CH_4 mole fraction. The quantitative observation of pseudoternary diagrams is consistent with both P–T and P–X diagrams for CO_2/CH_4 discussed previously.

3.1.3 CO_2/H_2S

When the acid gas in different proportions of CO_2 and H_2S is added into the Kash oil sample, Figure 16a illustrates the P–X phase behavior. Saturation pressures decrease gradually with increasing the acid gas mole fraction. All saturation pressures of acid gases are below pure CO_2

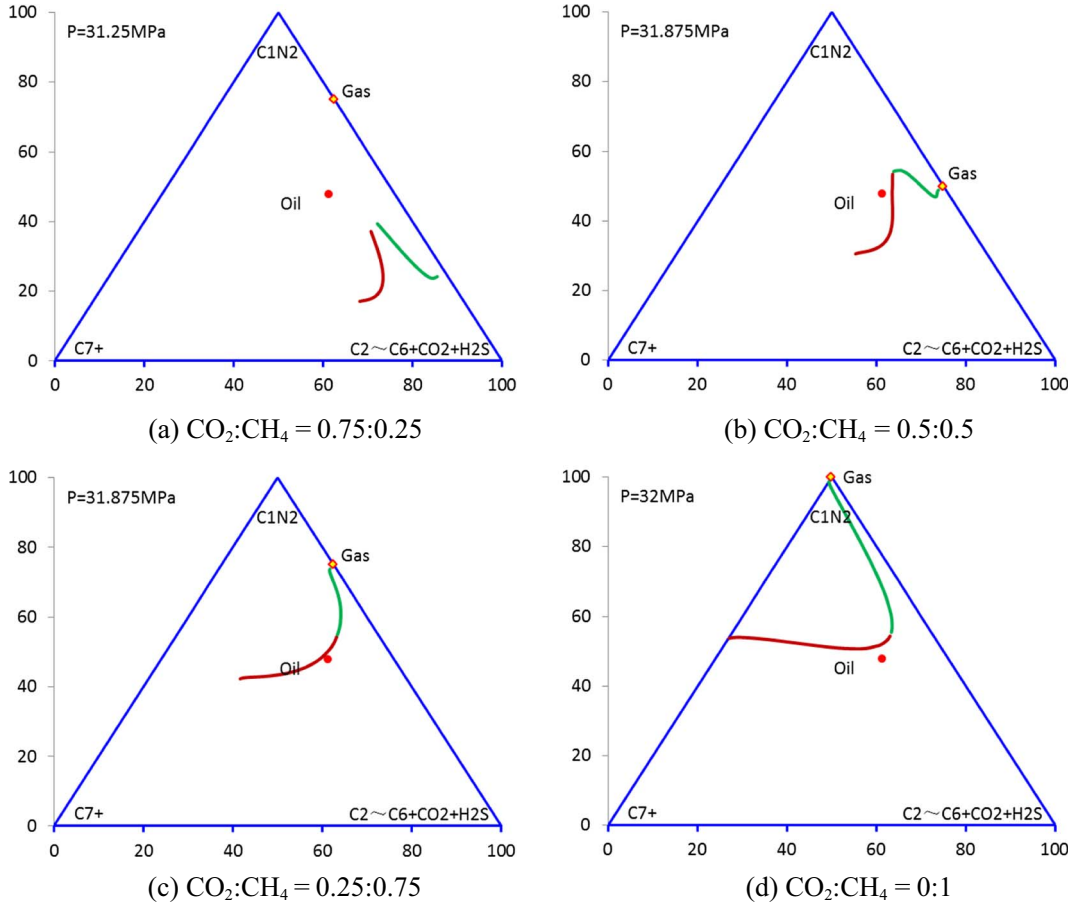

Fig. 15. Pseudoternary diagrams for Kash sour volatile oil sample at 109 °C with various CO_2/CH_4 mixtures as injection gas.

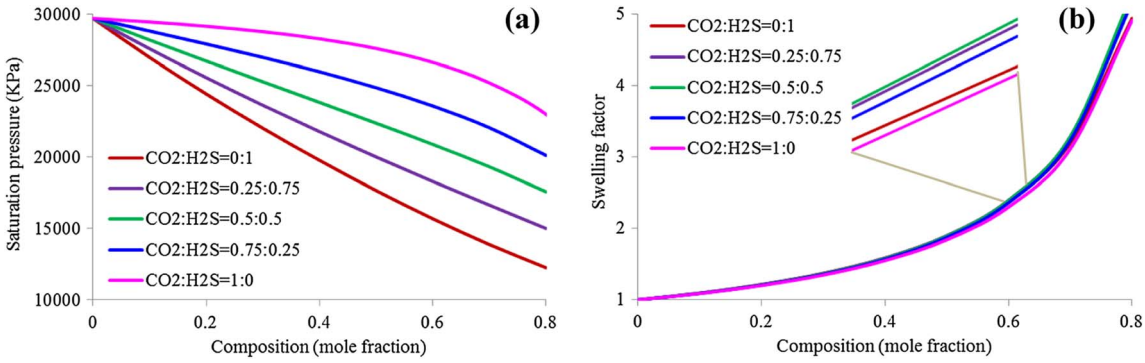

Fig. 16. (a) Pressure–composition diagrams and (b) swelling factors for Kash sour volatile oil and CO_2/H_2S mixtures at 109 °C.

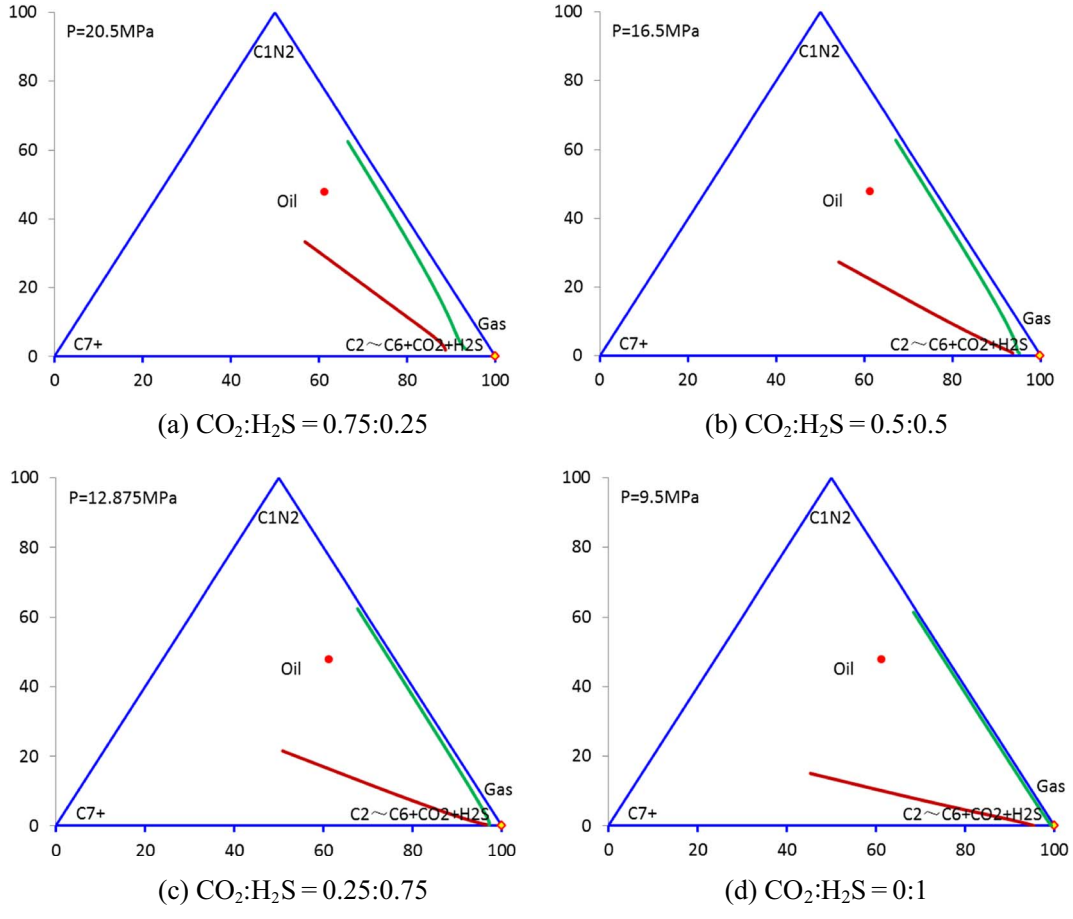

Fig. 17. Pseudoternary diagrams for Kash sour volatile oil sample at 109 °C with various CO_2/H_2S mixtures as injection gas.

saturation pressure curve, and FCM pressures cannot be seen. Moreover, it is found that the saturation pressure is the function of H_2S content. That is to say, the saturation pressure decreases linearly with an increase of H_2S concentration. It is to be recognized in the figure that H_2S is more preferential to achieve complete miscibility than CO_2. In general, the injected binary solvent CO_2/H_2S is easier to result in first-contact miscible or condensing gas drive. In Figure 16b, we can see that H_2S and CO_2 have almost identical swelling factors. However, the exhibiting trend of the swelling factor in CO_2/H_2S solvent differs slightly from CO_2/CH_4 and CO_2/N_2 solvents. The swelling factor does not follow the monotonic relationship with H_2S content increasing. The solvent of 0.5 mol CO_2 and 0.5 mol H_2S mixed with the reservoir oil exhibits the largest swelling factor. Practically it is difficult to be explained because of

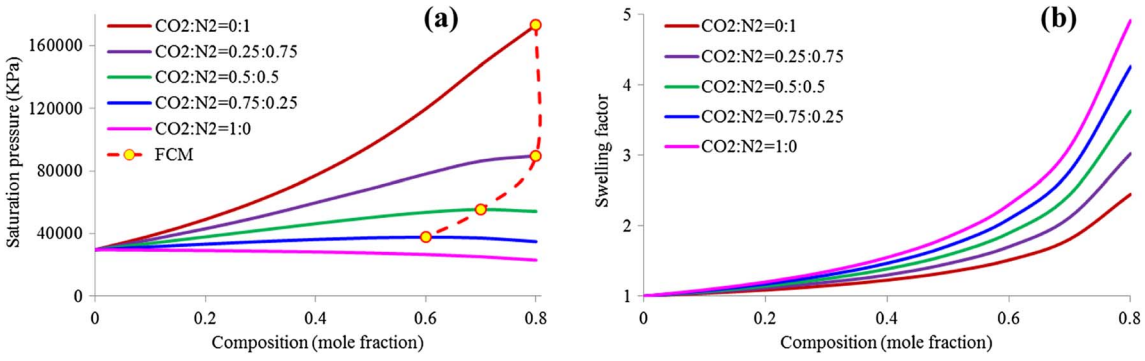

Fig. 18. (a) Pressure-composition diagrams and (b) swelling factors for Kash sour volatile oil and CO_2/N_2 mixtures at 109 °C.

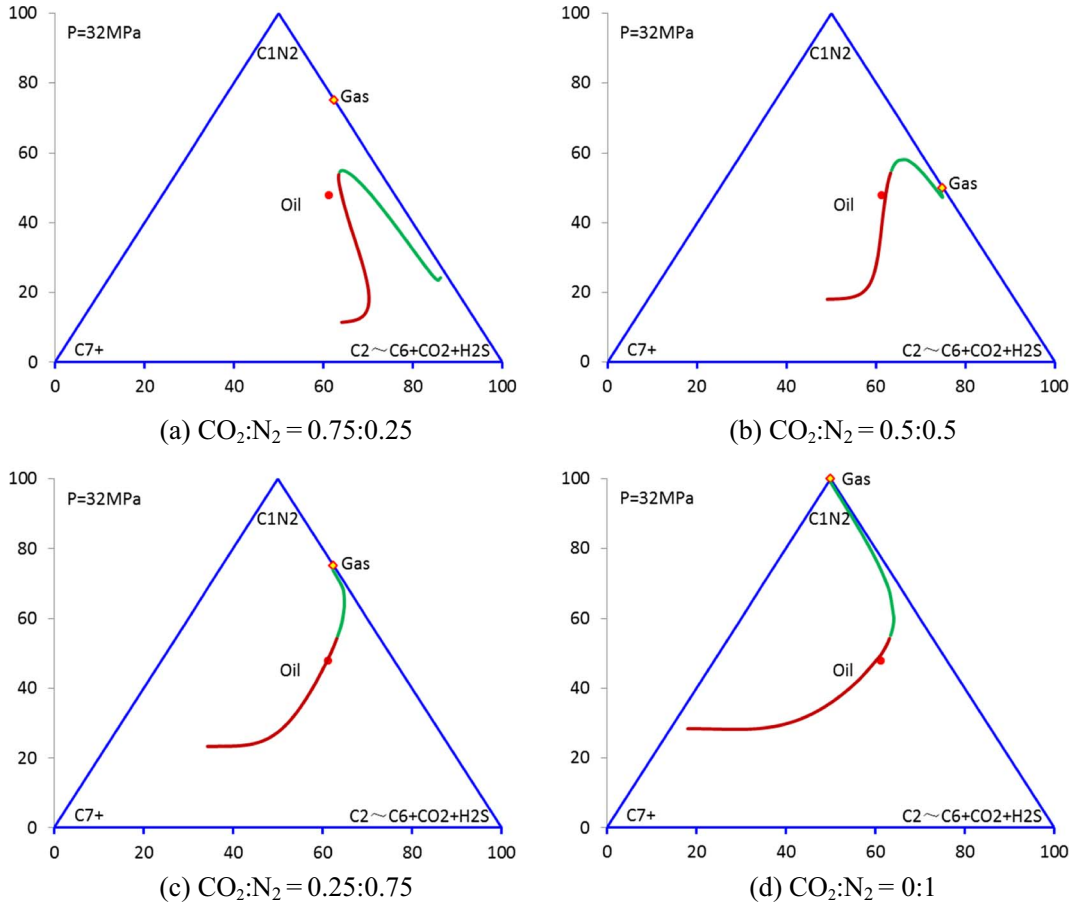

Fig. 19. Pseudoternary diagrams for Kash sour volatile oil sample at 109 °C with various CO_2/N_2 mixtures as injection gas.

complex phase behavior. All simulation results indicate that H_2S is substantially more effective than CO_2 in miscible development. Of course, safety considerations play a major importance role in acid gas injection processes.

Figure 17 shows the results of pseudoternary diagrams for the Kash oil with various CO_2/H_2S mixtures. The shape of phase envelope is like that of pure CO_2. The triangle area is expanded with increasing H_2S concentration but the MCM pressure decreases quickly. The result that H_2S is more favorable to miscibility development is consistent with the simulation observation of swelling test. For pure H_2S, the MCM pressure is determined to be 9.5 MPa. The increase of H_2S concentration in the injected CO_2/H_2S solvent reduces the MCM pressure by 1.675 MPa per 0.1 mol.

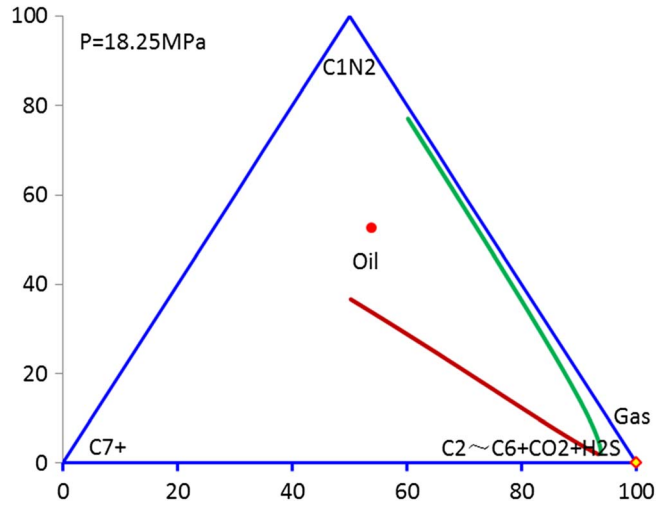

Fig. 20. Pseudoternary diagrams for Ken volatile oil sample at 91.7 °C with CO_2 as injection gas.

3.1.4 CO_2/N_2

For the flue gas containing different concentrations of CO_2 and N_2, mixed with the Kash oil, the P–X diagrams are shown in Figure 18a. Similarly, the shape of saturation pressure curves with the injection flue gas varies initially to go upward then downward. But FCM pressures of the N_2-rich system are far higher than the CH_4-rich system. In addition, the trend of swelling factor decreasing linearly with increasing N_2 concentration is also observed. Moreover, the maximum swelling factor of pure CO_2 is twice times as big as pure N_2 when the injected composition reaches 0.8 mol. Furthermore, it is found that the swelling factor of pure CH_4 is averaged 1.25 times as large as pure N_2 by comparison of Figures 13b and 18b. Based on all simulation results of swelling test, we can conclude that the relative order ranking of gas displacing the Kash oil to achieve miscible flooding is $H_2S > CO_2 > CH_4 > N_2$, which is consistent with analysis of the above P–T phase diagrams.

When N_2 is added to the CO_2 gas, the MCM pressure is kept constant at 32 MPa. The shape of phase boundary curves is identical to that of CO_2/CH_4 in Figure 19. But the area of two-phase region becomes larger. This figure implies that although the MCM pressure is the same, the moving path of the MCM process is different.

3.2 Evaluation on volatile oil

3.2.1 P–T consideration

The overall trend of pressure-temperature diagrams for the Ken volatile oil and CO_2 mixtures is highly analogous to

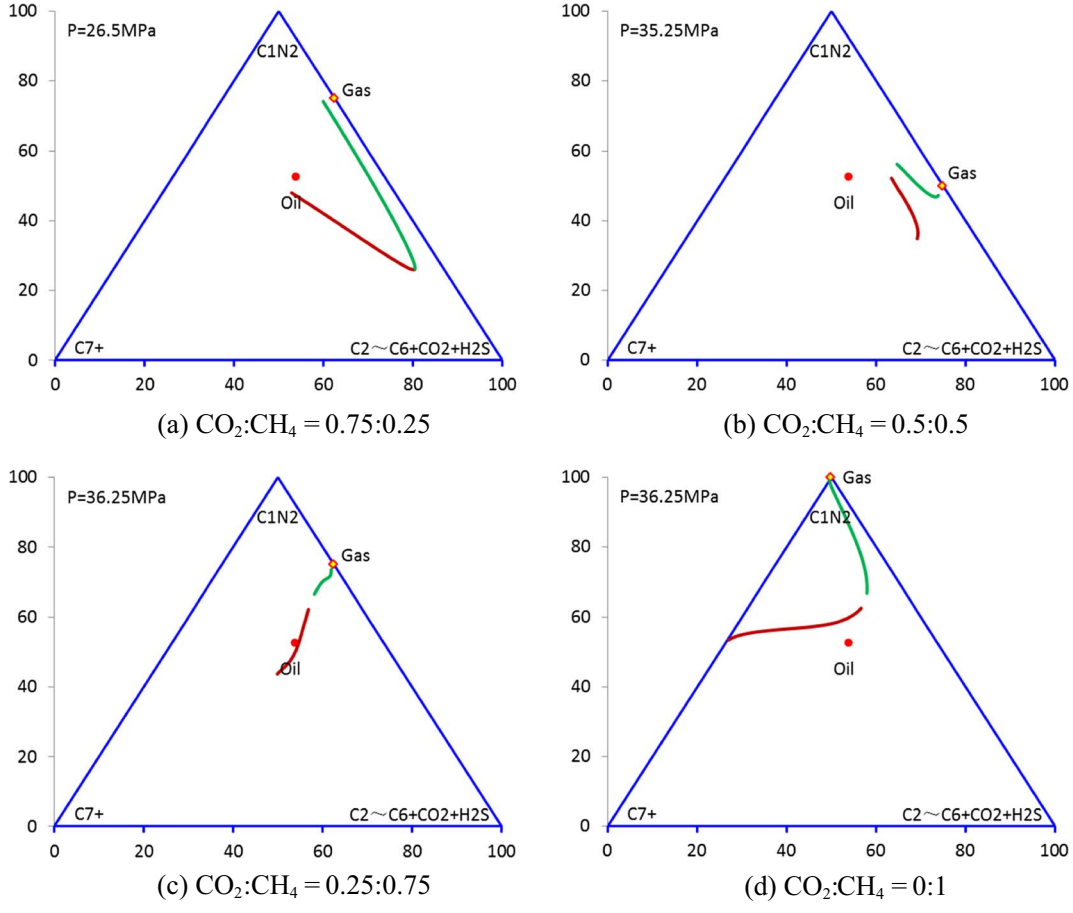

Fig. 21. Pseudoternary diagrams for Ken volatile oil sample at 91.7 °C with various CO_2/CH_4 mixtures as injection gas.

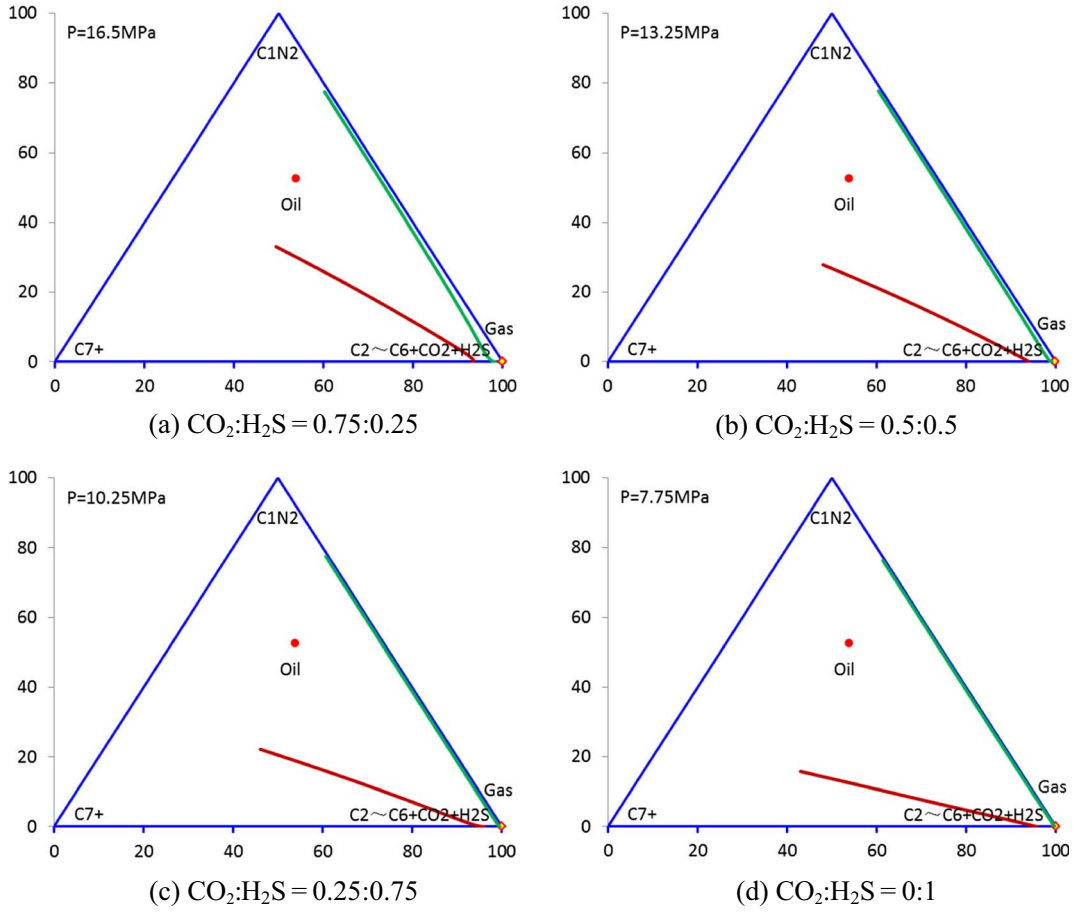

Fig. 22. Pseudoternary diagrams for Ken volatile oil sample at 91.7 °C with various CO_2/H_2S mixtures as injection gas.

the Kash oil. The small difference is these critical points of the Ken system are lower. The comparison of the four gases (H_2S, CO_2, CH_4 and N_2) mixed with the Ken oil on the P–T diagram is also very similar to the Kash oil. To avoid repeatedly, the two P–T diagrams are not presented.

3.2.2 CO_2/CH_4

For the Ken volatile oil mixed with CO_2/CH_4, the pressure-composition diagrams are similar to the Kash oil contacted with CO_2/CH_4 presented in Figure 13a. The main difference is FCM pressures of the Ken mixture system is higher than the Kash mixture system. This is reflected by the Kash oil high content of H_2S and CO_2 up to 19%. That is to say, H_2S and CO_2 existing in crude oil compositions are beneficial to achieve miscibility with reduced FCM pressures. Another pronounced difference is that the saturation pressure curve in the Ken mixture system does not distribute equally like the Kash mixture system, when the injected solvent is consisted of 0.75 mol CO_2 and 0.25 mol CH_4. The explanation can be drawn that the Ken oil contains more heavy hydrocarbons than the Kash sample, and more CO_2 gas can heavily extract C5–C30 fraction. Actually the process at 91.7 °C may be a liquid–liquid extraction and the CO_2 condensation would be dominant (Metcalfe and Yarborough 1979). However, all maximum swelling factor points in the Ken oil are smaller than that of the Kash oil, which indicates the swelling capability of the Ken crude oil is weak. Because the heavy component in the Ken oil (19.9 mol C7+) is higher compared with the Kash oil (14.7 mol C7+).

Figure 20 shows pseudoternary diagrams for the Ken volatile oil sample at 91.7 °C with pure CO_2 as injection gas. We should note the differences in the shape of phase envelope and the size of two-phase region between the Ken case and Kash case in Figure 14. The apex of the triangle shape for the former is completely closed. On the other hand, the bigger area of two-phase region is a result of lower MCM pressure (18.25 MPa). As CO_2 continues to be added to the Ken oil, both bubble point and dew point curves are slowly approaching to the intermediate pseudocomponent end as expected. The simulated results indicate a condensing-dominant/vaporizing process rather than a pure condensation.

Figure 21 shows the effect of CH_4 on the CO_2 drive for the Ken oil on the pseudoternary diagrams. An increase in the amount of CH_4 in the injected solvent would increase the MCM pressures. However, the MCM pressure would

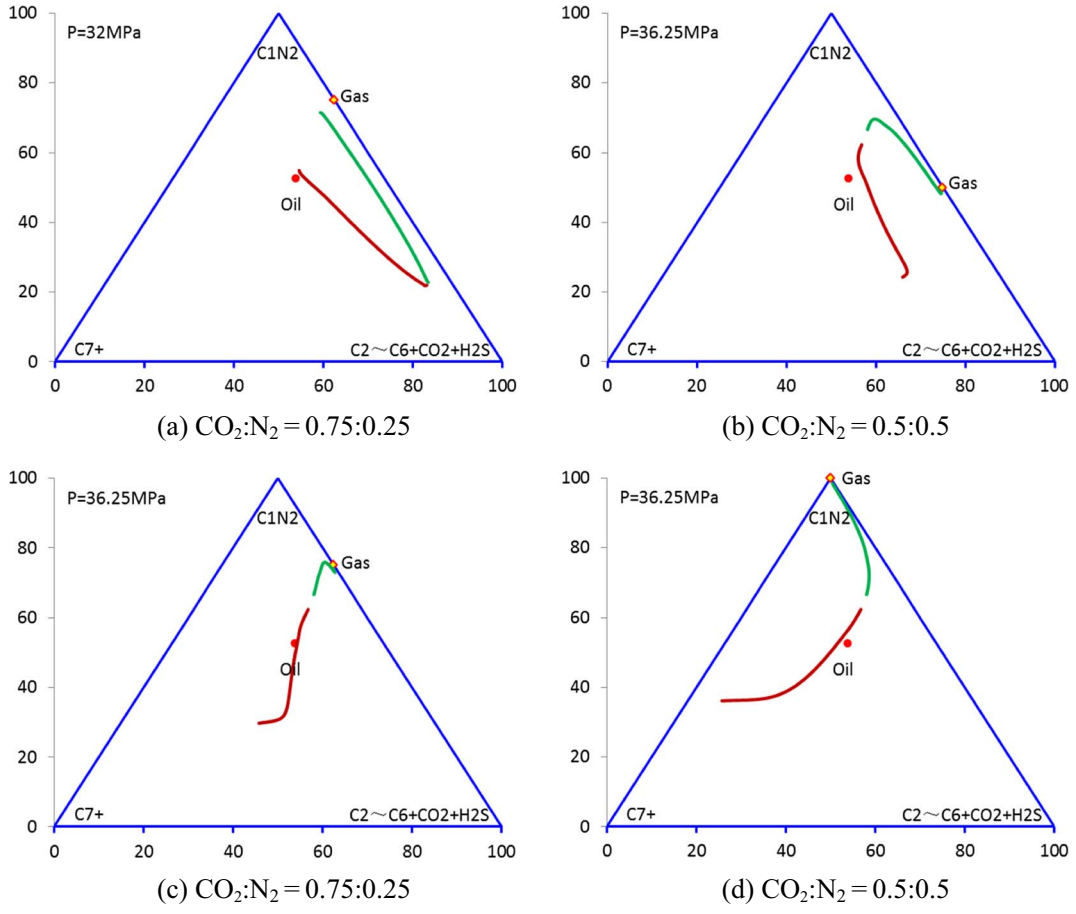

Fig. 23. Pseudoternary diagrams for Ken volatile oil sample at 91.7 °C with various CO_2/N_2 mixtures as injection gas.

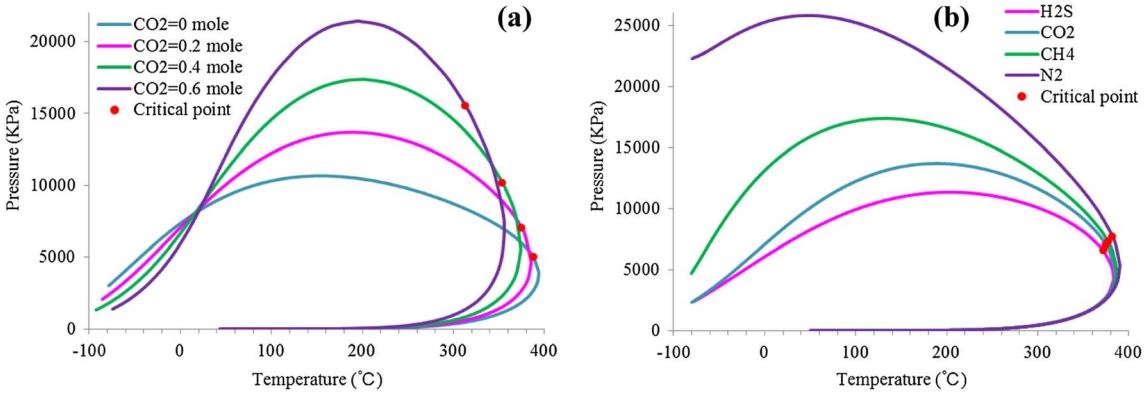

Fig. 24. Pressure–temperature diagrams for Jilin black oil with (a) CO_2 mixtures and (b) various injected gases.

keep a constant value of 36.25 MPa with CH_4 concentration larger than 0.75 mol. For pure CH_4, the estimated MCM pressure is determined to be 36.25 MPa, almost twice as large as that of pure CO_2. The four shapes of phase envelope are totally different with each other.

3.2.3 CO_2/H_2S

The overall trend of P–X diagrams for the Ken oil mixed with CO_2/H_2S of composition alteration is very analogous to Figure 16a. But the solvent of 0.75 mol CO_2 and 0.25 mol H_2S has maximum saturation pressure points and is

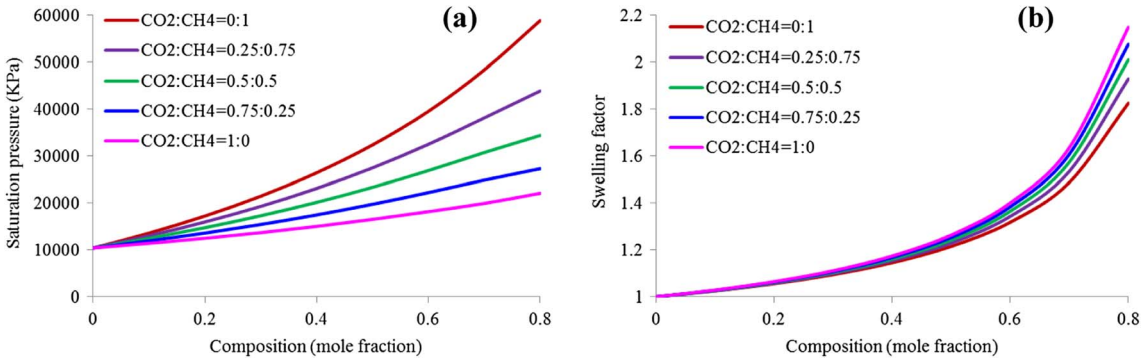

Fig. 25. (a) Pressure–composition diagrams and (b) swelling factors for Jilin black oil and CO_2/CH_4 mixtures at 108.4 °C.

unusual. The explanation is also tremendously difficult. H_2S in a sense is acting like CO_2 for a given pressure and temperature condition. Additional investigation is required. The swelling factor plots for Ken volatile oil sample at 91.7 °C is also similar to Figure 16b.

Figure 22 shows pseudoternary diagrams for the Ken oil with various CO_2/H_2S mixtures. An increase in the amount of H_2S in the injected solvent would decrease the MCM pressures as expected. For pure H_2S, the estimated MCM pressure is determined to be 7.75 MPa. The four shapes of phase envelope exhibit a triangle shape. The increase of H_2S concentration in the injected CO_2/H_2S solvent reduces the MCM pressure by 1.05 MPa per 0.1 mol.

3.2.4 CO_2/N_2

The P–X diagrams for Ken volatile oil and CO_2/N_2 mixtures at 91.7 °C are highly identical to Figure 18a for the Kash oil. On the basis of all simulation results of swelling test in the Ken oil, the miscibility of gas ($H_2S > CO_2 > CH_4 > N_2$) is typically consistent with the Kash oil.

Figure 23 shows pseudoternary diagrams for the Ken oil with various CO_2/N_2 mixtures. An increase in the amount of N_2 in the injected solvent would increase the MCM pressures. However, the MCM pressure would keep a constant value of 36.25 MPa with N_2 content larger than 0.5 mol. For pure N_2, the estimated MCM pressure is determined to be 36.25 MPa, with the same value of pure CH_4. The four shapes of phase envelope exhibit different shapes with each other.

3.3 Evaluation on black oil

3.3.1 P–T consideration

The Jilin black oil behaves totally different shape of phase envelope when CO_2 is added in Figure 24a. As CO_2 mole fraction is increased, the two-end of phase boundary becomes retractable but the middle part is expanded. The critical point shifts upward. This figure indicates that the oil composition plays a key role in the change of phase behavior. And the difference between black oil and volatile oil is quite clearly. All the bubble point curves of injection gases exhibit a downward trend in the low temperature region in Figure 24b.

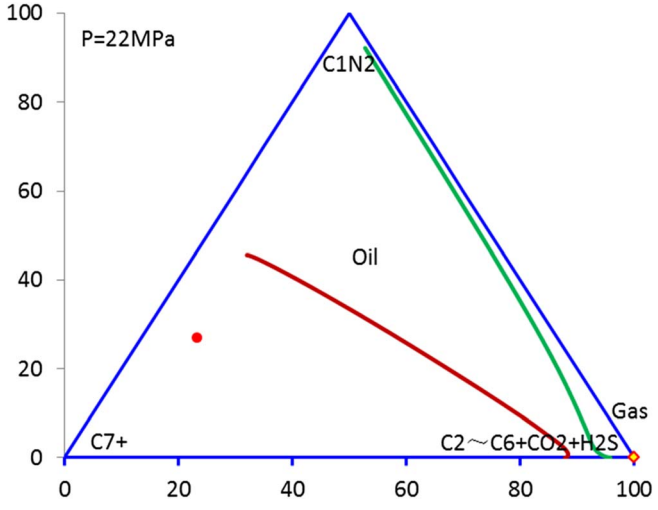

Fig. 26. Pseudoternary diagrams for Jilin black oil sample at 108.4 °C with CO_2 as injection gas.

3.3.2 CO_2/CH_4

For the Jilin black oil, as CO_2/CH_4 solvent is added to the reservoir oil, mixture saturation pressure increases steadily shown in Figure 25a, and FCM pressures disappear because the cricondenbar in this situation becomes impractically high. In practice, the black oil is difficult to achieve directly FCM. Dynamic miscibility may happen by the vaporizing gas drive mechanism of multiple contacts. The swelling factor for the Jilin oil almost is as half as the volatile oil as shown Figure 25b. Because the C7+ mole fraction for the black oil is on average 3.7 times as much as the volatile oil.

For pure CO_2 displacing the Jilin black oil, Figure 26 shows the behavior of pseudoternary diagrams of three pseudocomponents. The shape of phase boundary is basically analogous to those of the Kash and Ken systems.

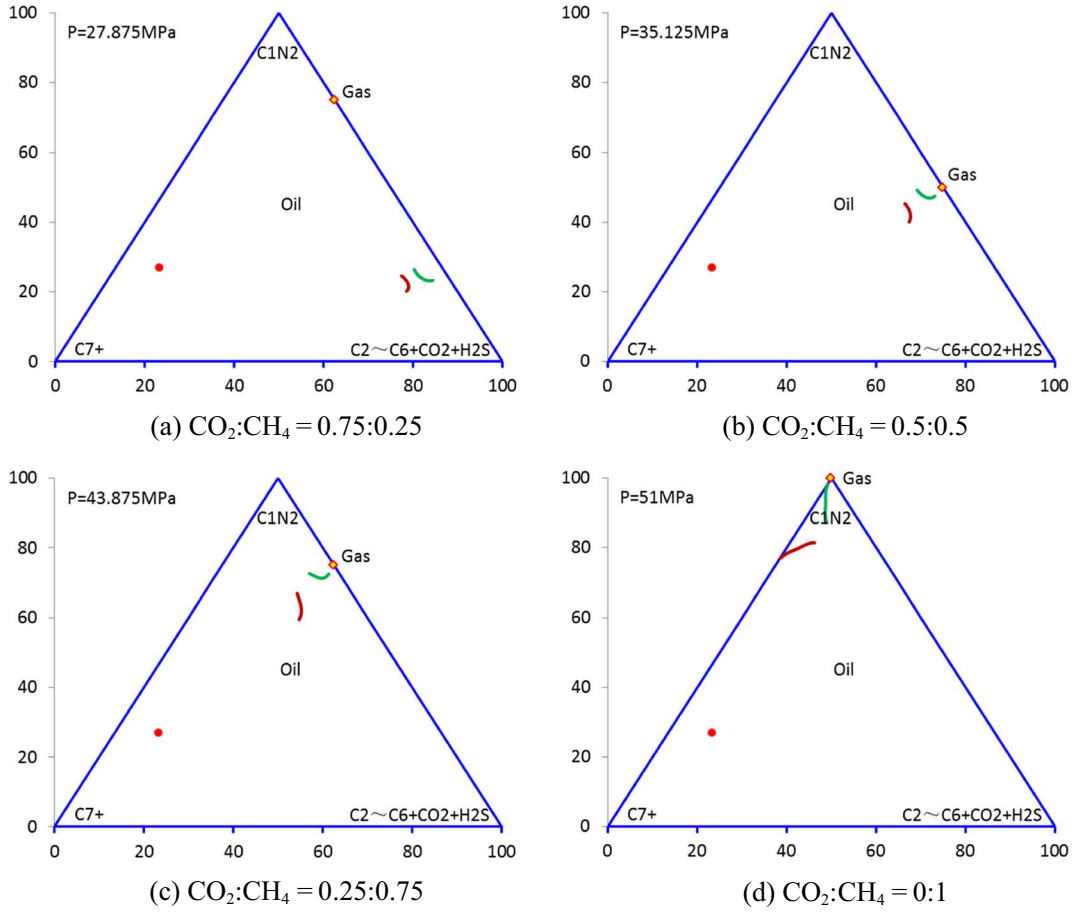

Fig. 27. Pseudoternary diagrams for Jilin black oil sample at 108.4 °C with various CO_2/CH_4 mixtures as injection gas.

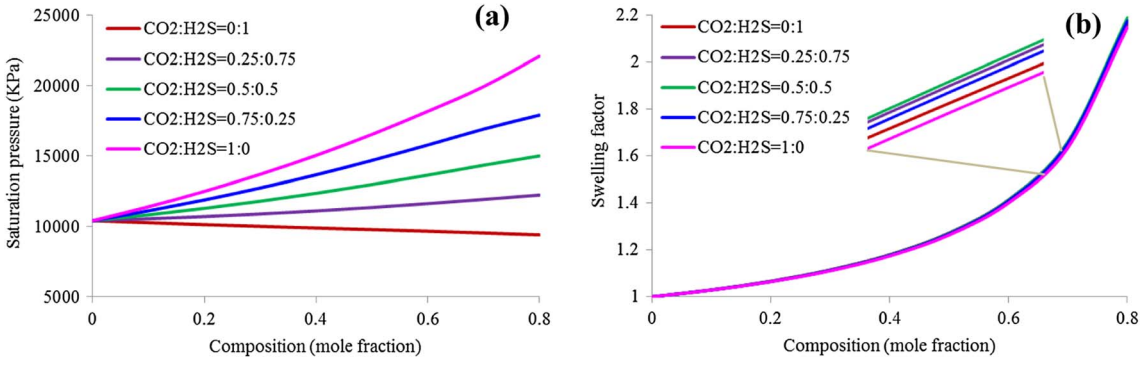

Fig. 28. (a) Pressure–composition diagrams and (b) swelling factors for Jilin black oil and CO_2/H_2S mixtures at 108.4 °C.

The MCM pressure of 22 MPa lies between the Kash and Ken mixed with pure CO_2. However, the area of two-phase region for the black oil is the largest among three systems. Besides the effect of temperature at the range of 91.7–109 °C, the displacement behavior depends on pressure and composition as expected. A sequence of displacement simulations are run to investigate the effect of CH_4 on CO_2 displacement mechanism. The calculated results are summarized in Figure 27. An increase in the amount of CH_4 in the injected solvent would raise the MCM pressures by 2.9 MPa per 0.1 mol. The shape of phase envelope exhibits a trump shape except a triangle shape of pure CH_4.

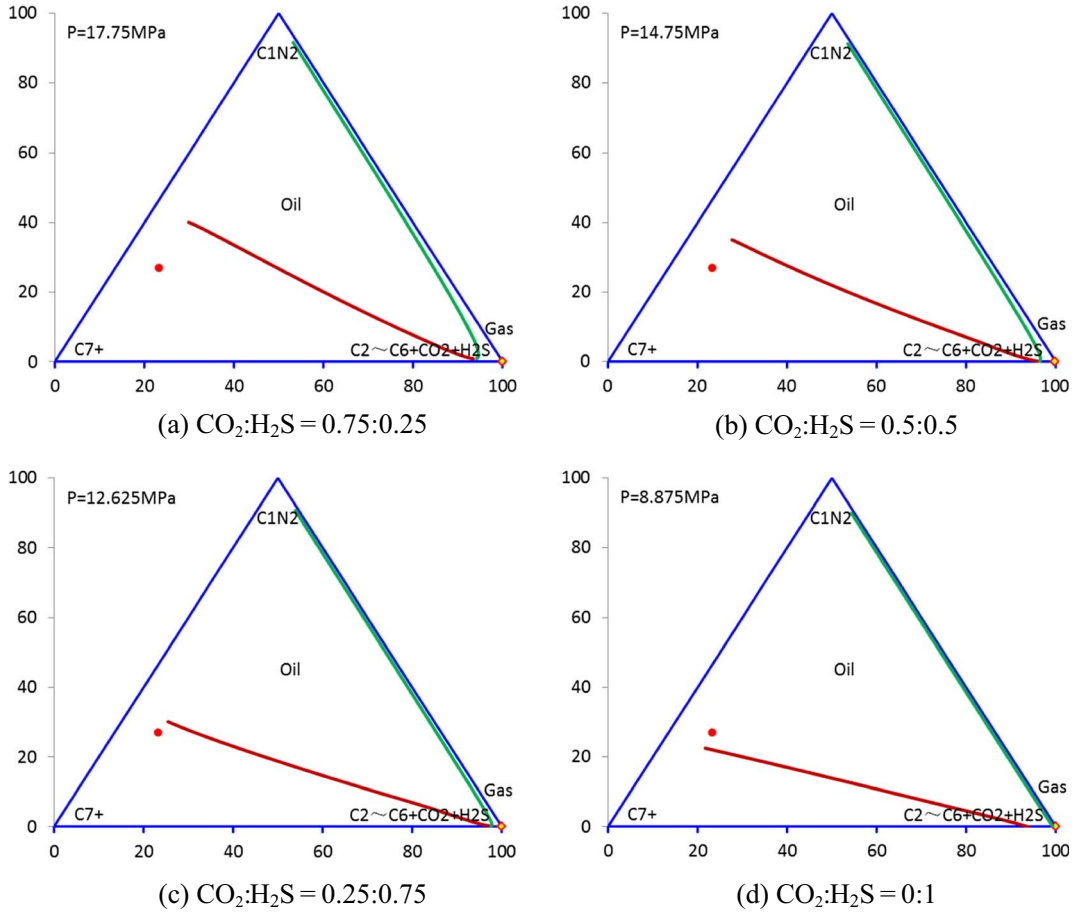

Fig. 29. Pseudoternary diagrams for Jilin black oil sample at 108.4 °C with various CO_2/H_2S mixtures as injection gas.

3.3.3 CO_2/H_2S

Unlike the decreasing trend of saturation pressure curves of the volatile oil, the black oil exhibits an increasing trend of saturation pressure with increasing CO_2/H_2S solvent as shown in Figure 28a. It is surprising that the swelling factor in the Jilin oil has the same feature of the Kash oil in Figure 28b. Unfortunately, the reasonable explanation of this phenomenon is still quite difficult.

Figure 29 shows pseudoternary diagrams for the Jilin oil with CO_2/H_2S. An increase in the amount of H_2S in the injected solvent would decrease the MCM pressures by 1.3125 MPa per 0.1 mol. The shape of phase envelope is quite consistent with those of the Kash in Figure 17 and Ken in Figure 22 systems, typically a triangle shape.

3.3.4 CO_2/N_2

According to P–X diagrams for Jilin black oil and CO_2/N_2 mixtures at 108.4 °C, it is very similar to the volatile oil of the Kash and Ken fluid system. However, FCM pressures do not be seen on the P–X diagram. Also, the swelling factor plot has identical feature. For the black oil, the miscibility ranking of four pure gases is consistent with the volatile oil, but the magnitude of miscibility is smaller because of composition alteration than that of the volatile oil.

Figure 30 shows pseudoternary diagrams for the Jilin oil with various CO_2/N_2 mixtures. An increase in the amount of N_2 in the injected solvent would increase the MCM pressures. However, the MCM pressure would keep a constant value of 79.25 MPa with N_2 content larger than 0.75 mol. The four shapes of phase envelope exhibit different shapes each other.

Figure 31 compares MCM pressures for various mixtures of CO_2/CH_4, CO_2/H_2S and CO_2/N_2 with three oils. A black line is set around 30 MPa. Above the line, all displacement processes are vaporizing gas drive. Below the line, a condensing-dominated gas drive would happen. It is evident that the binary mixtures CO_2/CH_4 and CO_2/N_2 can yield larger MCM pressure while CO_2/H_2S has smaller MCM pressure. Further comparison of MCM pressures for three oils mixed with CO_2/N_2, it is easily found that MCM pressures of pure N_2 for the Jilin system is twice greater than those of the Kash and Ken systems.

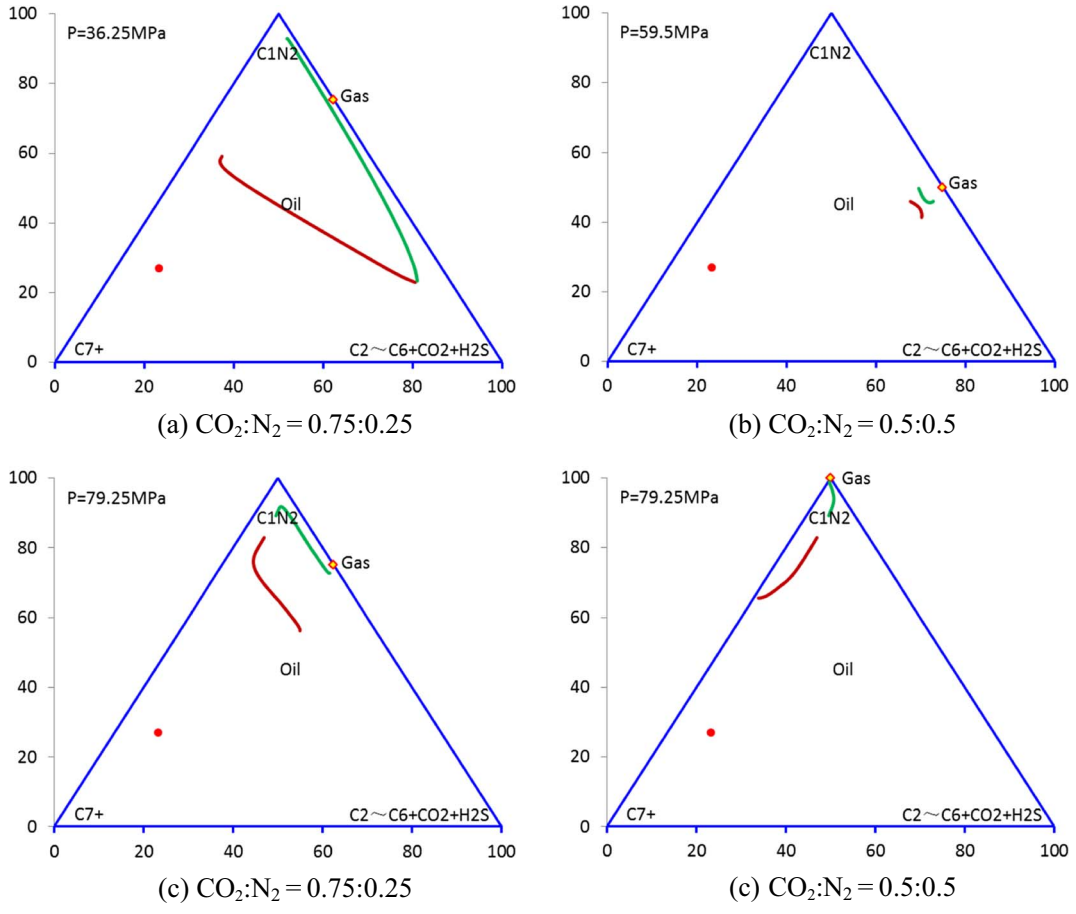

Fig. 30. Pseudoternary diagrams for Jilin black oil sample at 108.4 °C with various CO_2/N_2 mixtures as injection gas.

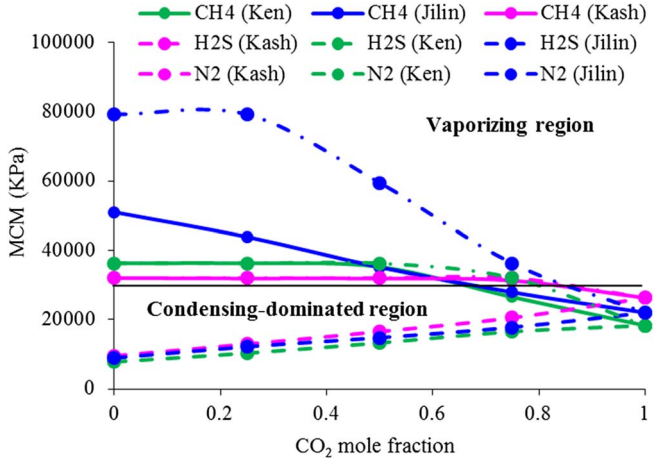

Fig. 31. MCM pressures for various mixtures of CO_2/CH_4, CO_2/H_2S and CO_2/N_2.

4 Conclusion

Three nine-pseudocomponent models have been established to predict the change of phase behavior and the type of miscible displacement mechanisms. The purpose of PVT experiments matching is to verify the compositional simulation model and guarantee a satisfactory prediction. Based on the accurate description of the fluid model from three real fields, the effects of impurity containing CH_4, H_2S and N_2 on miscible CO_2-EOR are investigated on the use of three tools with P–T diagram, P–X diagram and pseudoternary diagram. The major findings of the simulated results are summarized as follows:

1. Both CO_2 and H_2S are able to reduce effectively the MCM pressure, with the MCM pressure of pure H_2S for three reservoir fluids below 10 MPa. Conversely, both CH_4 and N_2 increase the MCM pressure and the maximum value reaches about 80 MPa, requiring a higher pressure to achieve miscible displacement.
2. For three oil samples, the binary mixtures of CO_2/H_2S during the MCM process belong basically to the condensation-dominated region, while most CO_2/CH_4 and CO_2/N_2 are developed by the MCM of vaporization. This result indicates that the type of displacement mainly depends on the nature of the injected gas rather than crude oil compositions.
3. From the simulation of swelling test, both CO_2 and H_2S decrease the saturation pressure while CH_4 and N_2 raise it. Moreover the swelling capability of H_2S is equivalent to CO_2, but both of them are higher than CH_4, and N_2 is the smallest one.

4. The volatile oil of the Kash and Ken oils contains the intermediate component of C2–C6 more than the black oil of the Jilin oil. So the change of P–T diagrams behaves different characteristics as the injected solve is added, and the variant magnitude of FCM and MCM pressures and swelling factors also exhibits differently.
5. Although only considering the binary mixtures in our work, the mixtures of two and three pure gases with CO_2 can also gain a quick evaluation according to the proposed procedure. The dominant gas would exert a decisive influence on miscible CO_2-EOR.

Acknowledgments. The authors greatly acknowledge the financial support from the Important National Science and Technology Specific Projects of China (No. 2017ZX05030-002 and No. 2016ZX05016-001).

References

Abdurrahman M., Permadi A.K., Bae W.S. (2015) An improved method of estimating minimum miscibility pressure through condensation-extraction process under swelling tests, *J. Pet. Sci. Eng.* **131**, 165–171.

Abou-Sayed A.S., Zaki K., Summers C. (2004) Management of sour gas by underground injection – Assessment, challenges and recommendations. SPE-86605.

Abrishami Y., Hatamian H. (1996) Phase behaviour of fluids in multiple contact processes with CO_2, N_2 and their mixture. SPE-36295.

AlFalahy M.A., Abou-Kassem J.H., Chakma A., Islam M.R., Al-Ain U.A.E. (1998) Sour gas processing, disposal, and utilization as applied in UAE reservoirs. SPE-49504.

Al-Wahaibi Y.M., Muggeridge A.H., Grattoni C.A. (2007) Experimental and numerical studies of gas/oil multicontact miscible displacements in homogeneous and crossbedded porous media, *SPE J.* **12**, 01, 62–76.

Babadagli T. (2007) Development of mature oil fields – A review, *J. Pet. Sci. Eng.* **57**, 3–4, 221–246.

Bachu S., Gunter W.D. (2005) Overview of acid-gas injection operations in western Canada, *Greenh. Gas. Control. Technol.* **1**, 443–448.

Bahralolom I.M., Orr F.M. Jr. (1988) Solubility and extraction in multiple-contact miscible displacements: Comparison of N_2 and CO_2 flow visualization experiments, *SPE Reserv. Eng.* **3**, 01, 213–219.

Battistelli A., Marcolini M. (2009) TMGAS: A new TOUGH2 EOS module for the numerical simulation of gas mixtures injection in geological structures, *Int. J. Greenh. Gas. Control* **3**, 481–493.

Behrend J., Chugh S., Mckishnie R.A. (2007) Development of the Strasshof Tief sour-gas field incluing acid-gas injection into adjacent producing sour-gas reservoirs, *SPE Reserv. Eval. Eng.* **10**, 05, 572–579.

Belhaj H., Abukhalifeh H., Javid K. (2013a) Miscible oil recovery utilizing N_2 and/or HC gases in CO_2 injection, *J. Pet. Sci. Eng.* **111**, 144–152.

Belhaj H., Khalifeh H.A., Javid K. (2013b) Potential of nitrogen gas miscible injection in South East assets, Abu Dhabi. SPE-164774.

Chapoy A., Nazeri M., Kapateh M., Burgass R., Coquelet C., Tohidi B. (2013) Effect of impurities on thermophysical properties and phase behaviour of a CO_2-rich system in CCS, *Int. J. Greenh. Gas. Control* **19**, 92–100.

Coats K.H., Thomas L.K., Pierson R.G. (2007) Simulation of miscible flow including bypassed oil and dispersion control, *SPE Reserv. Eval. Eng.* **10**, 05, 500–507.

Fandino O., Trusler J.P.M., Vega-Maza D. (2015) Phase behavior of (CO_2 + H_2) and (CO_2 + N_2) at temperatures between (218.15 and 303.15) K at pressures up to 15 MPa, *Int. J. Greenh. Gas. Control* **36**, 78–92.

Firoozabadi A., Aziz K. (1986) Analysis and correlation of nitrogen and lean-gas miscibility pressure, *SPE Reserv. Eng.* **1**, 06, 575–582.

Han H.S., Li S., Chen X.L., Qin J.S., Zeng B.Q. (2016) Main control factors of carbon dioxide on swelling effect of crude hydrocarbon components, *Acta Petrol. Sin.* **37**, 03, 392–398.

Hand J.L., Pinczewskl W.V. (1990) Interpretation of swelling/extraction tests, *SPE Reserv. Eng.* **5**, 4, 595–600.

Harvey A.H., Henry R.L. (1960) A laboratory investigation of oil recovery by displacement with carbon dioxide and hydrogen sulfide. SPE-6983.

He C.G., Mu L.X., Xu A.Z., Zhao L., He J., Zhang A.G., Shan F.C., Luo E.H. (2019) Phase behavior and miscible mechanism in the displacement of crude oil with associated sour gas, *Oil Gas Sci. Technol. - Rev. IFP Energies nouvelles* **74**, 54.

Holm L.W., Josendal V.A. (1974) Mechanisms of oil displacement by carbon dioxide, *J. Petrol. Technol.* **26**, 12, 1427–1438.

Huang N.S., Aho G.E., Baker B.H., Matthews T.R., Pottorf R.J. (2011) Integrated reservoir modeling of a large sour-gas field with high concentrations of inerts, *SPE Reserv. Eval. Eng.* **14**, 4, 418–432.

Jaubert J.N., Avaullee L., Zaborowski G. (1995) Characterization of heavy oils. 3. Prediction of gas injection behavior: Sweeling test, multicontact test, multiple-contact minimum miscibility pressure, and multiple-contact minimum miscibility enrichment, *Ind. Eng. Chem. Res.* **34**, 4016–4032.

Jaubert J.N., Privat R., Le Guennec Y., Coniglio L. (2016) Note on the properties altered by application of a Peneloux-type volume translation to an equation of state, *Fluid Phase Equilib.* **419**, 88–95.

Jin L., Pekot L.J., Bhathorne S.B., Salako O., Peterson K.J., Bosshart N.W., Jiang T., Hamling J.A., Gorecki C.D. (2018) Evaluation of recycle gas injection on CO_2 enhanced oil recovery and associated storage performance, *Int. J. Greenh. Gas. Control* **75**, 151–161.

Le Guennec Y., Lasala S., Privat R., Jaubert J.N. (2016a) A consistency test for α-functions of cubic equations of state, *Fluid Phase Equilib.* **427**, 513–538.

Le Guennec Y., Privat R., Jaubert J.N. (2016b) Development of the translated-consistent tc-PR and tc-RK cubic equations of state for a safe and accurate prediction of volumetric, energetic and saturation properties of pure compounds in the sub- and super-critical domains, *Fluid Phase Equilib.* **429**, 301–312.

Li H., Jakobsen J.P., Wilhelmsen O., Yan J. (2011) PVTxy properties of CO_2 mixtures relevant for CO_2 capture, transport and storage: Review of available experimental data and theorecical models, *Appl. Energy* **88**, 3567–3579.

Li H., Yan J. (2009) Impacts of equations of state (EOS) and impurities on the volume calculation of CO_2 mixtures in the applications of CO_2 capture and storage (CCS) processes, *Appl. Energy* **86**, 2730–2770.

Longworth H.L., Dunn G.C., Semchuck M. (1996) Underground disposal of acid gas in Alberta, Canada: Regulatory concerns and case histories. SPE-35584.

Luo E.H., Fan Z.F., Hu Y.L., Zhao L., Zhao H.Y., Wang J.J., He C.G., Zeng X. (2019a) A dual-porosity dual-permeability model for acid gas injection process evaluation in hydrogen-carbonate reservoir, *Int. J. Hydrogen. Energy* **44**, 25169–25179.

Luo E.H., Fan Z.F., Hu Y.L., Zhao L., Wang J.J. (2019b) An evaluation on mechanisms of miscibility development in acid gas injection for volatile oil reservoirs, *Oil Gas Sci. Technol. - Rev. IFP Energies nouvelles* **74**, 59.

Luo E.H., Hu Y.L., Li B.Z., Zhu W.P. (2013a) Practices of CO_2 EOR in China, *Special Oil Gas Reserv.* **20**, 2, 1–7. (in Chinese).

Luo E.H., Hu Y.L., Li B.Z., Wang J.L., Wang Z.B. (2013b) Methods of improving sweep volume by mobility control of CO_2 flood in foreign countries, *Oilfield Chem.* **30**, 4, 613–619. (in Chinese).

Luo P., Er V., Freitag N., Huang S. (2013c) Recharacterizing evolving fluid and PVT properties of Weyburn oil-CO_2 system, *Int. J. Greenh. Gas. Control* **16S**, S226–S235.

McGuire P.L., Okuno R., Gould T.L., Lake L.W. (2017) Ethane-based enhanced oil recovery: An innovative and profitable enhanced-oil-recovery opportunity for a low-price environment, *SPE Reserv. Eval. Eng.* **20**, 01, 42–58.

Metcalfe R.S., Yarborough L. (1979) The effect of phase equilibria on the CO_2 displacement mechanism, *Soc. Pertrol. Eng. J.* **19**, 4, 242–252.

Mohsen-Nia M., Moddaress H., Mansoori G.A. (1993) Sour natural gas and liquid equationo of state. SPE-26906.

Neau E., Jaubert J.N., Rogalski M. (1993) Characterization of heavy oils, *Ind. Eng. Chem. Res.* **32**, 1196–1203.

Newley T.M.J., Merrill R.C. Jr (1991) Pseudocomponent selection for compositional simulation, *SPE Reserv. Eng.* **6**, 4, 490–496.

Nutakki R., Hamoodi A.N., Li Y.-K., Nghiem L.X. (1991) Experimental analysis, modelling, and interpretation of recovery mechanisms in enriched-gas processes. SPE-22634.

Onerhime A., Kveps A., Daher E. (2014) Addressing safety challenges of operating in sour gas fields: A case study from the Middle East. SPE-170393.

Privat R., Jaubert J.N., Le Guennec Y. (2016) Incorporation of a volume translation in an equation of state for fluid mixtures: Which combining rule? Which effect on properties of mixing? *Fluid Phase Equilib.* **427**, 414–420.

Rahimi V., Bidarigh M., Bahrami P. (2017) Experimental study and performance investigation of miscible water-alternating-CO_2 flooding for enhancing oil recovery in the Sarvak formation, *Oil Gas Sci. Technol. - Rev. IFP Energies nouvelles* **72**, 35.

Siddiqui M., Baber S., Saleem W.A., Jafri M.O., Hafeez Q. (2013) Industry practices of sour gas management by reinjection: Benefits, methodologies, economic evaluation and case studies. SPE-169645.

Simon R., Graue D.J. (1964) Generalized correlations for predicting solubility, swelling and viscosity behavior of CO_2-crude oil systems, *J. Petrol. Technol.* **17**, 1, 102–106.

Spivey J.P., McCain W.D. (2013) Estimating reservoir composition for gas condensates and volatile oils from field data. SPE-166414.

Srivastava R.K., Huang S.S. (1997) Comparative effectiveness of CO_2, produced gas, and flue and gas for enhanced heavy oil recovery. SPE-37558.

Stalkup F.I. (1987) Displacement behavior of the condensing/vaporizing gas drive process. SPE-16715.

Trivedi J.J., Babadagli T., Lavoie R.G., Nimchuk D. (2005) Acid gas sequenstration during teriary oil recovery: Optimal injection strategies and importance of operational parameters, *J. Can. Petrol. Technol.* **46**, 3, 1–17.

Tsau J.S., Bui L.H., Willhite G.P. (2010) Swelling/extraction test of a small sample size for phase behavior study. SPE-129728.

Vark W.V., Masalmeh S.K., Dorp J.V., Nasr M.A.A., Al-Khanbashi S. (2004) Simulation study of miscible gas injection for enhanecd oil recovery in low permeable carbonate reservoirs in Abu Dhabi. SPE-88717.

Verlaan C., Zwet G. (2012) Challenges and opportunities in sour gas developments. SPE-162167.

Wang G.C. (1986) A study of crude oil composition during CO_2 extraction process. SPE-15085.

Yang S.L., Hang D.Z., Sun R., Lv W.F., Wu M., Deng H. (2009) CO_2 extraction for crude oil and its effect on crude oil viscosity, *J. China Univ. Petrol.* **33**, 4, 85–88.

Ziabakhsh-Ganji Z., Kooi H. (2012) An equation of state for thermodynamic equilibrium of gas mixtures and brines to allow simulation of the effects of impurities in subsurface CO_2 storage, *Int. J. Greenh. Gas. Control* **11S**, S21–S34.

Zick A.A. (1986) A combined condensing/vaporizing mechanism in the displacement of oil by enriched gases. SPE-15493.